OXFORD

Human Molecular Genetics, 2018, Vol. 27, No. 16 2874–2892

doi: 10.1093/hmg/ddy201
Advance Access Publication Date: 30 May 2018
Original Article

ORIGINAL ARTICLE

Benfotiamine treatment activates the Nrf2/ARE pathway and is neuroprotective in a transgenic mouse model of tauopathy

Victor Tapias[1], Shari Jainuddin[1], Manuj Ahuja[2], Cliona Stack[1], Ceyhan Elipenahli[1], Julie Vignisse[3], Meri Gerges[1], Natalia Starkova[1], Hui Xu[1], Anatoly A. Starkov[1], Lucien Bettendorff[3], Dmitry M. Hushpulian[4,5], Natalya A. Smirnova[4], Irina G. Gazaryan[6,7], Navneet A. Kaidery[2], Sushama Wakade[2], Noel Y. Calingasan[1], Bobby Thomas[2], Gary E. Gibson[1,8], Magali Dumont[1] and M. Flint Beal[1,*]

[1]Brain and Mind Research Institute, Weill Cornell Medicine, New York, NY 10065, USA, [2]Department of Pharmacology, Toxicology and Neurology, Augusta University, Augusta, GA 30912, USA, [3]Laboratory of Neurophysiology, GIGA-Neurosciences, University of Liege, 4000 Liege, Belgium, [4]D. Rogachev Federal Scientific and Clinical Center for Pediatric Hematology, Oncology, and Immunology, 117997 Moscow, Russia, [5]Veropharm, Abbott EPD, 115088 Moscow, Russia, [6]Department of Chemistry and Physical Sciences, Pace University, Pleasantville, NY 10570, USA, [7]Department of Enzymology, School of Chemistry, 119991 Moscow, Russia and [8]Burke Medical Research Institute, Weill Cornell Medicine, White Plains, NY 10605, USA

*To whom correspondence should be addressed at: Weill Cornell Medicine, Brain and Mind Research Institute, 525 East 68th Street, New York, NY 10065, USA. Tel: +1 2127466546; Fax: +1 2127468276; Email: fbeal@med.cornell.edu

Abstract

Impaired glucose metabolism, decreased levels of thiamine and its phosphate esters, and reduced activity of thiamine-dependent enzymes, such as pyruvate dehydrogenase, alpha-ketoglutarate dehydrogenase and transketolase occur in Alzheimer's disease (AD). Thiamine deficiency exacerbates amyloid beta (Aβ) deposition, tau hyperphosphorylation and oxidative stress. Benfotiamine (BFT) rescued cognitive deficits and reduced Aβ burden in amyloid precursor protein (APP)/PS1 mice. In this study, we examined whether BFT confers neuroprotection against tau phosphorylation and the generation of neurofibrillary tangles (NFTs) in the P301S mouse model of tauopathy. Chronic dietary treatment with BFT increased lifespan, improved behavior, reduced glycated tau, decreased NFTs and prevented death of motor neurons. BFT administration significantly ameliorated mitochondrial dysfunction and attenuated oxidative damage and inflammation. We found that BFT and its metabolites (but not thiamine) trigger the expression of Nrf2/antioxidant response element (ARE)-dependent genes in mouse brain as well as in wild-type but not Nrf2-deficient fibroblasts. Active metabolites were more potent in activating the Nrf2 target genes than the parent molecule BFT. Docking studies showed that BFT and its metabolites (but not thiamine) bind to Keap1 with high affinity. These findings demonstrate that BFT activates the Nrf2/ARE pathway and is a promising

Received: March 22, 2018. **Revised:** April 26, 2018. **Accepted:** May 1, 2018

therapeutic agent for the treatment of diseases with tau pathology, such as AD, frontotemporal dementia and progressive supranuclear palsy.

Introduction

Thiamine (vitamin B1) plays a central role in brain energy metabolism. Thiamine diphosphate (ThDP) is an essential cofactor of alpha-ketoglutarate dehydrogenase complex, pyruvate dehydrogenase complex and transketolase. ThDP is the most abundant derivative in the brain and other tissues, while free thiamine and other phosphorylated derivatives (thiamine monophosphate, ThMP and thiamine triphosphate, ThTP) may be important for other brain functions (1–4). Accumulating evidence has demonstrated that thiamine deficiency plays a central role in the pathogenesis of neurodegenerative diseases, including Alzheimer's disease (AD) (5,6). A marked reduction in thiamine, its derivatives, and thiamine-dependent enzymes has been detected in plasma, red blood cells (5,7,8), cerebrospinal fluid (9), and postmortem brain tissue from AD patients (5,10–12).

There is an established correlation between the decrease of thiamine-dependent processes and the severity of dementia in AD subjects (13). Thiamine deficiency accelerated amyloid plaque deposition, increased amyloid beta $(A\beta)_{1-42}$, β-carboxyterminal fragment (C99) and BACE levels, and exacerbated oxidative stress and inflammation in Tg19959 transgenic (TG) mice overexpressing a double mutant form of the human amyloid precursor protein (APP) (14). Clinical trials of thiamine replacement, as a treatment in AD patients, however, were inconclusive, showing either a mild beneficial effect or no effect on cognition (15–17).

Oxidative stress is involved in the onset and progression of several neurodegenerative diseases, including AD (18,19). Thiamine deficiency mimics important aspects of oxidative stress in AD. Thiamine-deficient mice show elevated malondialdehyde and 3-nitrotyrosine and reduced catalase, superoxide dismutase (SOD) and glutathione peroxidase activities (20,21). Oxidative stress may result from several interconnected causes, such as mitochondrial dysfunction or inflammation, which are processes that occur in the brains of thiamine-deficient animals (22).

Benfotiamine (BFT) is a synthetic S-acyl derivative of thiamine with an open-ringed structure that enhances thiamine bioavailability by ∼5-fold as assessed by plasma levels (23). BFT prevents the formation of advanced glycation end products and has beneficial effects in experimental models of diabetic retinopathy, nephropathy and neuropathy (24,25). In APP/PS1 mice, BFT was reported to dose-dependently improve behavioral deficits and reduce amyloid deposition (26). It was reported that in the brains of mice treated with BFT there was an increase in phosphorylation of glycogen synthase kinase-3β (GSK-3β), which correlates with decreases in its activity. These authors reported that BFT decreased the number of phosphorylated tau-positive cells in APP/PS1 mice after 8-week treatment in a dose-dependent fashion. It, however, did not comment on neurofibrillary tangles (NFTs), which were not observed in the initial description of the APP/PS1 mice or in subsequent reports (27,28). It is therefore uncertain whether BFT reduces NFTs, which is an important issue since the cognitive deficits encountered in AD correlate better with numbers of NFTs, and loss of synapses than with amyloid plaques (29,30).

The development of therapeutic interventions targeting tau pathology in AD and frontotemporal dementia is of great interest. We therefore evaluated the neuroprotective effects of BFT in the P301S TG mouse model of tauopathy that overexpresses the human tau gene harboring the P301S mutation, which causes frontotemporal dementia in man (31,32). We observed neuroprotective effects and provide the first evidence that BFT and its metabolites activate the nuclear factor erythroid 2-related factor (Nrf2)/antioxidant response element (ARE) pathway.

Results

BFT treatment increases lifespan, ameliorates behavioral deficits, and attenuates neuronal death

To assess the effects of BFT on lifespan, a separate cohort of TG mice were fed with BFT or control diet until natural death. BFT-treated P301S TG mice lived significantly longer than their TG littermates fed with a control diet (average of 390 versus 322 days; 21% increase in longevity) (Fig. 1B), although no changes in body weight were observed (Fig. 1A). To study behavioral deficits, P301S TG mice were assessed at 5, 7 and 9 months of age using the elevated plus maze (EPM) (to assess anxiety-like behavior) (Fig. 1C) and at 9 months of age using the contextual fear conditioning (to assess associative fear learning and memory) (Fig. 1D). TG mice showed enhanced hyperactivity and disinhibition as well as memory impairment relative to WT mice. Nevertheless, these behavioral deficits were rescued in TG mice treated with BFT. During the training period, all mice were able to learn the task and freeze after two electric shocks. Hind limb paralysis is a distinctive feature of TG mice at late-stage disease (32,33). To determine the effects of BFT on cell death, L3–L6 regions of the spinal cord, which contain motor neuron pools for the hind limbs, were stained with cresyl violet and subjected to stereological neuron counting (Fig. 1E–G). The number of SMI32-positive neurons was also assessed (Fig. 1H–J). We found a significant preservation of motor neurons in TG mice treated with BFT relative to TG mice on a control diet.

Tau pathology is reduced following BFT administration

Tau pathology was assessed using an AT8 antibody that detects phosphorylated tau in NFTs (Fig. 2). A marked decrement in AT8 immunoreactivity, with a subsequent reduction in tau hyperphosphorylation, was detected in both the cerebral cortex (Fig. 2A; $1.26 \pm 0.44\%$ versus $0.46 \pm 0.07\%$ area, $P < 0.05$) and hippocampus (Fig. 2B; $5.53 \pm 1.44\%$ versus $2.17 \pm 0.76\%$ area, $P < 0.05$) of P301S TG mice treated with BFT relative to mice on a control diet. Owing to its involvement in tau phosphorylation, the protein levels of phosphorylated GSK-3β were also examined by western blot (26,34). No alterations were found in phospho-GSK-3β expression following BFT treatment in the brain cortical tissue homogenates of TG mice (Supplementary Material, Fig. S1).

BFT increases thiamine levels in both the CNS and periphery

Levels of thiamine and its phosphorylated derivatives were measured in the CNS (cerebral cortex and hippocampus), liver

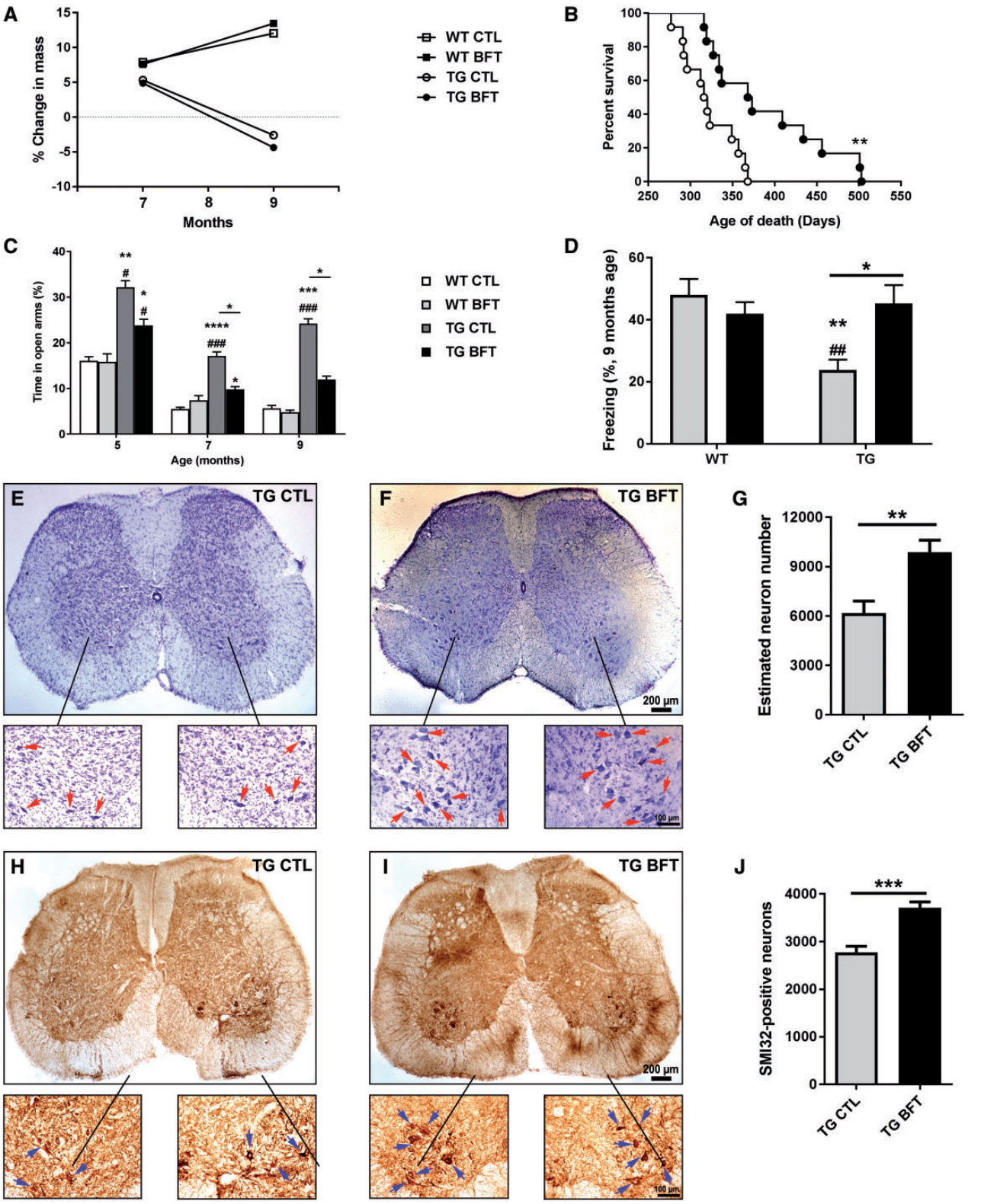

Figure 1. BFT treatment increased lifespan, improved behavioral deficits, and prevented motor neuron death in P301S mice. (**A**) Animal weight. No differences were observed following chronic BFT administration. (**B**) Survival curve. BFT-treated TG mice showed a significant increase in lifespan. $^{**}P < 0.01$ compared with TG CTL (Gehan–Breslow–Wilcoxon test). (**C**) EPM and (**D**) contextual fear conditioning. Long-term treatment with BFT enhanced memory and reduced behavioral hyperactivity and disinhibition. $^{****}P < 0.0001$, $^{***}P < 0.001$, $^{**}P < 0.01$ and $^{*}P < 0.05$ relative to WT CTL. $^{###}P < 0.001$, $^{##}P < 0.01$ and $^{#}P < 0.05$ versus WT BFT. $^{*}P < 0.05$ compared with TG CTL (two-way ANOVA followed by Tukey multiple comparisons test). L3–L6 regions of the spinal cord, which contain motor neuron pools for the hind limbs, were stained with cresyl violet (**E** and **F**) and the SMI32 antibody (**H** and **I**), which recognizes an epitope on non-phosphorylated neurofilament of proteins. Stereological counts show a higher number of motor neurons in BTF treated P301S TG mice compared with TG mice on a control diet. Quantitative analysis was carried out in eight sections per animal. Each treatment group was comprised of six mice. $^{**}P < 0.01$ and $^{*}P < 0.05$ relative to TG CTL (unpaired *t*-test). Scale bar: 200 µm at low magnification and 100 µm at high magnification.

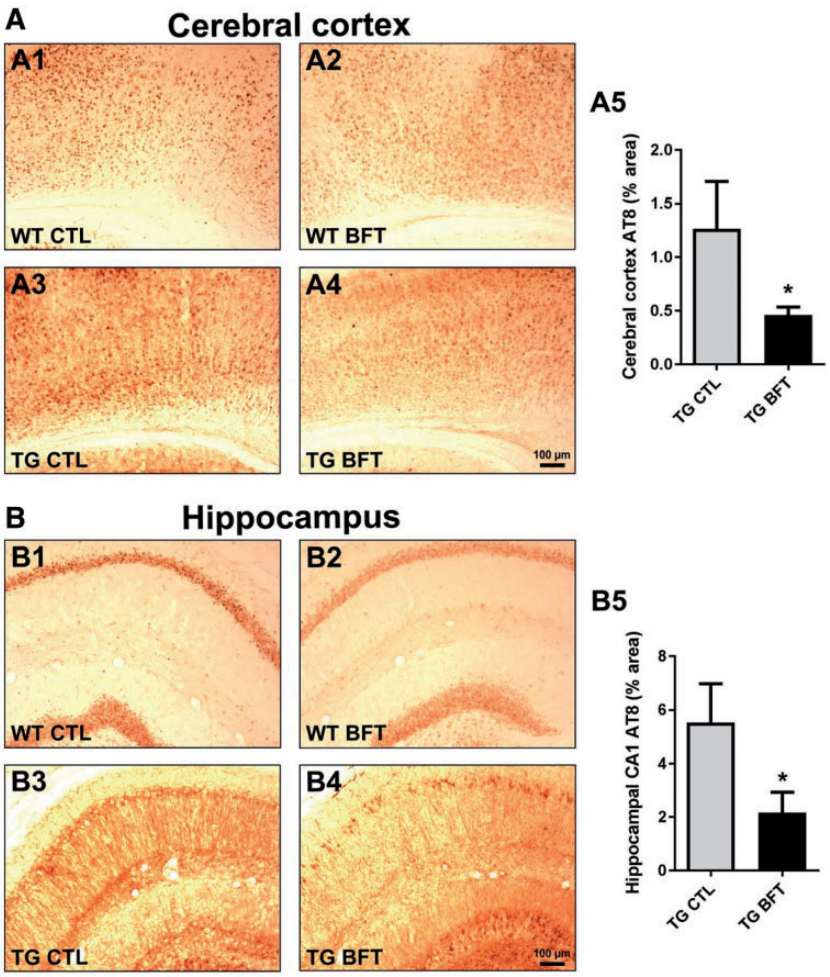

Figure 2. Reduced tau pathology following BFT administration. Immunostaining with AT8 antibody in the cerebral cortex (**A**) and hippocampus (**B**) of WT and TG mice treated with BFT or control diet. Calculation of the percent area occupied by AT8-immunopositive neurons revealed that BFT significantly reduced tau hyperphosphorylation in the brain of TG mice. For all tests, $n = 6$ for TG CTL and $n = 8$ for TG BFT. *$P < 0.05$ compared with TG CTL (unpaired *t*-test). Scale bar: 100 µm.

and blood of WT and TG 10-month-old mice (Fig. 3). In blood and liver, administration of BFT increased the levels of free thiamine, ThMP and ThDP (Fig. 3C and D). The brain levels of thiamine, ThMP and ThDP are much lower, and the brain response to BFT is much less than that in the blood and liver. Thiamine and ThMP levels were significantly elevated in the cerebral cortex and the hippocampus of WT mice while no changes were observed in TG mice (Fig. 3A and B). ThDP levels were variable among groups. Thiamine and its derivatives were also assessed in the spinal cord, but no differences occurred amongst the groups (data not shown).

BFT administration improves mitochondrial function

We examined whether BFT ameliorated mitochondrial dysfunction in P301S TG mice (Fig. 4). Thus, several important mitochondrial antioxidant enzymes were analyzed. Mitochondrial complex I protein levels were decreased in TG when compared with WT mice ($P < 0.05$) and treatment with BFT induced a marked increase in complex I immunoreactivity ($P < 0.01$) (Fig. 4A). The enzyme activity of the thiamine-dependent enzymes TK and α-KGDHC were also evaluated in the mouse cerebral cortex. TK activity was significantly reduced in TG mice receiving the control diet when compared with WT littermates (Fig. 4B; 9.9 ± 0.3 versus 7.4 ± 0.8 mU/mg protein, $P < 0.001$). The reduced TK levels were significantly increased in P301S TG mice after BFT treatment, restoring them to those seen in the control group (7.4 ± 0.8 versus 9.1 ± 0.3 mU/mg protein, $P < 0.05$). Though not statistically significant, there was a trend toward a higher α-KGDHC activity in TG mice treated with BFT relative to TG mice on the control diet (Fig. 4C). The SOD enzymatic activity was decreased by ∼50% in TG mice on the control diet while BFT long-term exposure increased the levels of SOD by ∼70% (Fig. 4D). Interestingly, the levels of PGC-1α were reduced in TG mice compared with WT littermates (∼85%) and BFT administration resulted in an upregulation of PGC-1α mRNA levels in P301S TG mice (Fig. 4E). There was a significant increase in the mtDNA copy number in P301S TG mice treated with BFT (Fig. 4F; $P < 0.05$), consistent with the finding that BFT increases PGC-1α levels and stimulates mitochondrial biogenesis.

The dynamin-related protein DRP1 is involved in mitochondrial fragmentation and abnormal mitochondrial dynamics in neurodegenerative diseases. Immunohistochemistry revealed higher DRP1 immunoreactivity in motor neurons in the ventral horn of the lumbar spinal cord of untreated TG mice relative to WT littermates. Administration of BFT diminished DRP1 expression in P301S TG mice (Fig. 4G). Complex II activity and the expression of the non-thiamine dependent mitochondrial

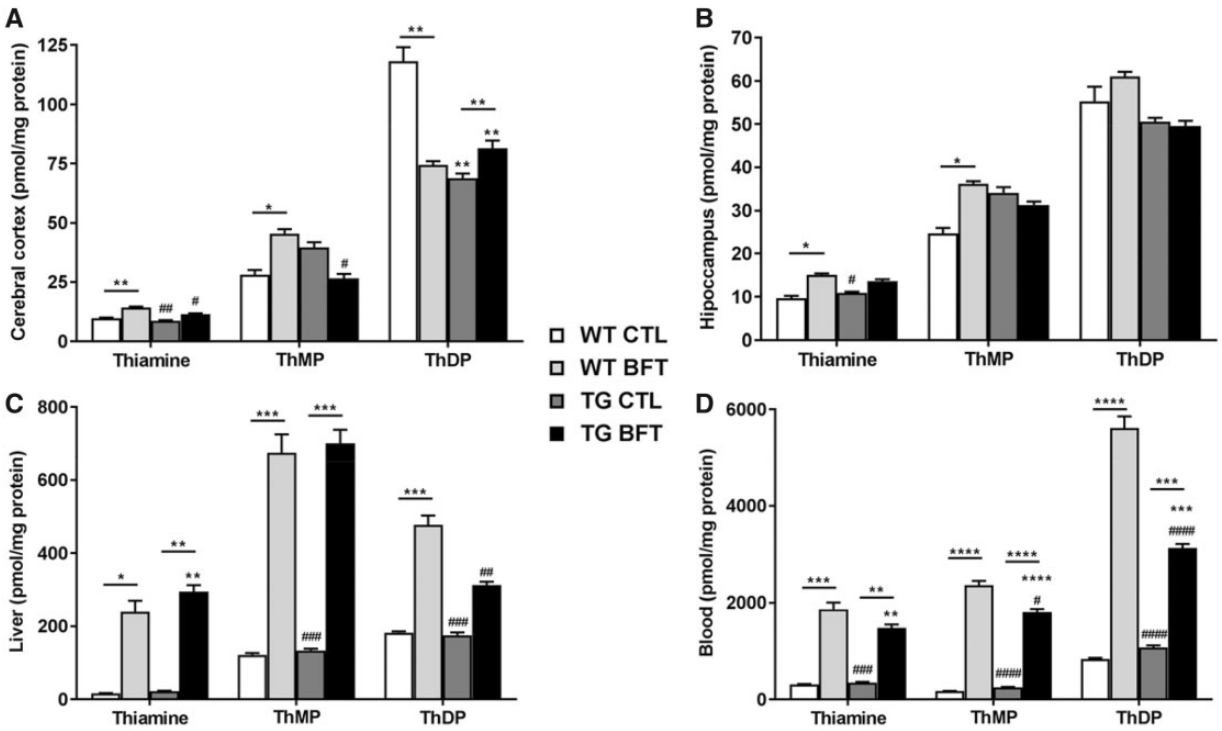

Figure 3. Levels of thiamine and its metabolites. Content of thiamine, ThMP and ThDP levels in the cerebral cortex (**A**), hippocampus (**B**), liver (**C**) and blood (**D**) of WT and TG mice. Treatment with BFT resulted in elevated levels of thiamine, ThMP and ThDP in the liver and blood of both WT littermates and P301S TG mice. However, BFT only increases the concentration of cortical and hippocampal thiamine, ThMP and ThDP in WT mice but remained unchanged in TG mice. The experimental groups were comprised of seven mice for CTL group and eight mice for BFT group. $^{****}P < 0.0001$, $^{***}P < 0.001$, $^{**}P < 0.01$ and $^{*}P < 0.05$ versus WT CTL. $^{\#\#\#\#}P < 0.001$, $^{\#\#\#}P < 0.001$, $^{\#\#}P < 0.01$ and $^{\#}P < 0.05$ compared with WT BFT. $^{****}P < 0.0001$, $^{***}P < 0.001$ and $^{**}P < 0.01$ relative to TG CTL (two-way ANOVA followed by Tukey multiple comparisons test).

electron transport chain enzyme Complexes III, IV and F_oF_1 ATP synthase remained unaltered by BFT treatment in either TG or WT mice (Supplementary Material, Fig. S2A–D, respectively). No significant alterations were observed in either citrate synthase (CS) activity (the initial enzyme of the TCA cycle) or TFAM mRNA levels (a transcription factor for mtDNA) after BFT treatment (Supplementary Material, Fig. S2E and F).

BFT treatment reduced advanced glycation end products

To evaluate advanced glycation end products (AGEs), tissue sections were immunostained using an antibody directed against carboxymethyl lysine (CML), one of the most abundant and well-established AGEs (Fig. 5). CML immunoreactivity was significantly enhanced in the CNS and motor neurons of the lumbar spinal cord of non-treated P301S TG mice compared with WT CTL mice. Quantitative analysis revealed that BFT treatment significantly decreased CML expression in the cerebral cortex (Fig. 5A5), hippocampus (Fig. 5B5) and spinal cord (Fig. 5C5) of TG mice.

Long-term exposure to BFT reduces oxidative and nitrosative stress

To assess oxidative damage, spinal cord sections were stained using antibodies that specifically recognize 3-NT (to evaluate protein tyrosine nitration) and 4-HNE (to examine lipid peroxidation) (35,36). Immunofluorescent micrographs at 40x depicted a faint 3-NT fluorescence signal (Supplementary Material, Figs S3A2 and A6) and weak 4-HNE staining (Supplementary Material, Figs S3A3 and A7) in the motor neurons (anti-choline acetyltransferase antibody ChAT) of WT mice. The staining for 3-NT and 4-HNE was significantly increased in TG mice (Fig. 6A2 and A3). BFT administration led to a significant reduction in the fluorescence signal for both 3-NT and 4-HNE (Fig. 6A6 and A7) and was quantified for 3-NT (Fig. 6B, $P < 0.05$) and 4-HNE (Fig. 6C, $P < 0.01$).

SOD-1 is the intracellular SOD which reduces the superoxide of the mitochondrial intermembrane space and cytosol to H_2O_2, whereas SOD-2 is found within mitochondria. SOD1-derived H_2O_2 functions as a second messenger to regulate various signal transduction pathways involved in inflammation. In this study, we examined the endogenous protein levels of cytosolic SOD-1 (Fig. 6D and S3B). Confocal analysis revealed a significant decrease in SOD-1 immunoreactivity in the spinal cord motor neurons of TG mice while BFT treatment significantly elevated SOD-1 levels (Fig. 6E; 40 ± 3 versus 49 ± 2 fluorescence units, $P < 0.05$).

Thioredoxin genes are also important for protection against oxidative stress. Cytosolic TRX-1 deficiency could contribute to enhanced oxidative damage and neuronal degeneration in AD. Our results demonstrated that chronic exposure to BFT caused a significant increase in TRX-1 mRNA levels in P301S TG mice relative to TG mice on the control diet (Fig. 6F; 0.9 ± 0.03 versus 1.2 ± 0.05-fold change, $P < 0.01$). NQO1 is a cytosolic flavoprotein that catalyzes the two-electron reduction of quinones and derivates, protecting against ROS production. Exposure to BFT upregulated the mRNA levels of NQO1 in TG mice (Fig. 6G; 0.89 ± 0.14 versus 1.61 ± 0.21-fold change, $P < 0.05$).

To further assess oxidative damage, levels of protein carbonyls, a standard marker of oxidative damage to proteins, were determined in the cerebral cortex of the P301S TG mice (Supplementary

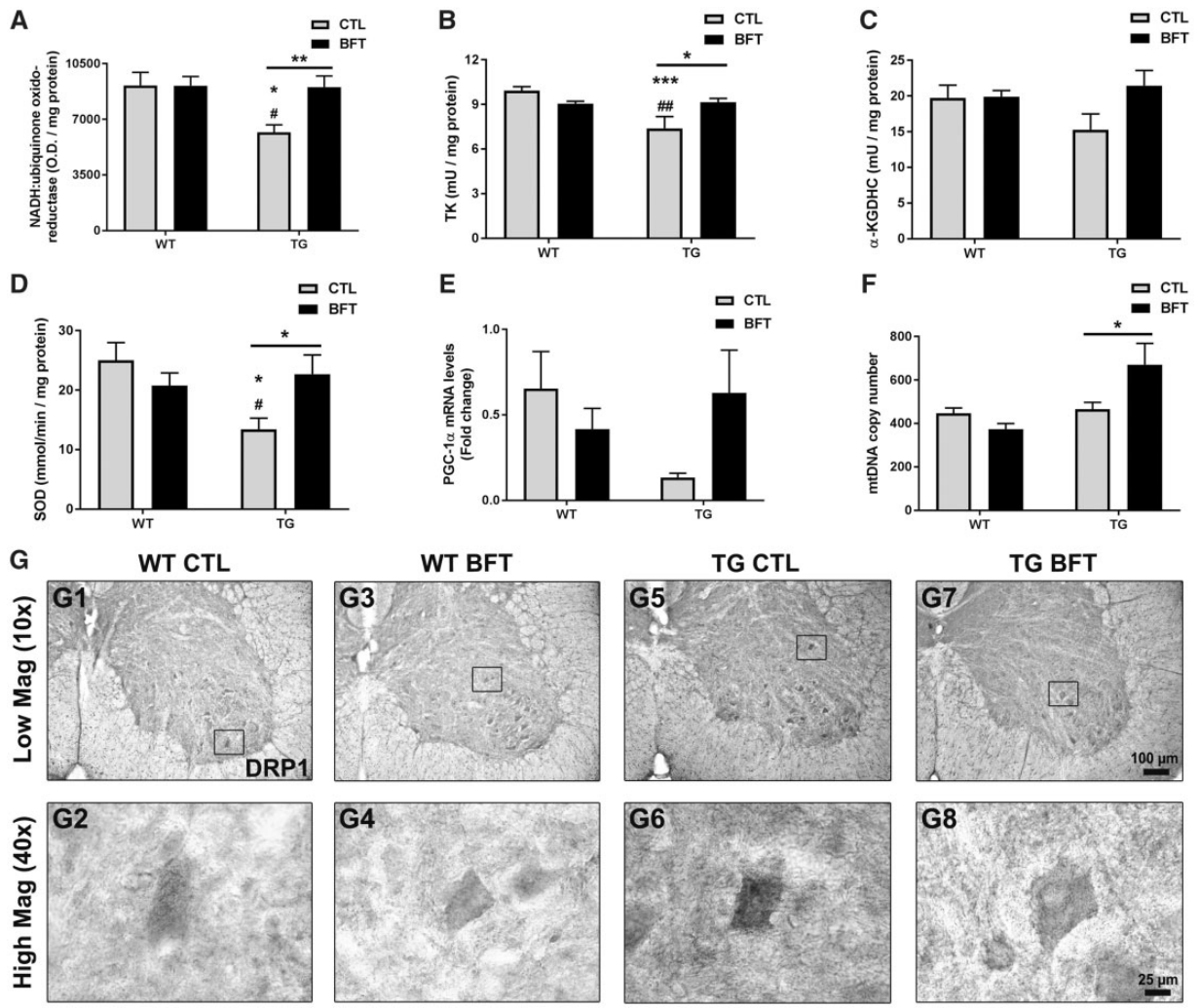

Figure 4. BFT restores mitochondrial dysfunction. Frontal lobe samples were used to determine the mitochondrial expression of complex I (**A**), enzymatic activity of TK (**B**), α-KGDHC (**C**) and SOD (**D**), mRNA levels of PGC-1α (**E**), and mtDNA copy number (**F**). TG mice fed BFT exhibited a considerable increase in Complex I immunoreactivity, enzymatic activities, PGC-1α levels and the copy number of mtDNA. Data are mean ± S.E.M. of six to eight mice per group. $^{***}P < 0.001$ and $^{*}P < 0.05$ relative to WT CTL. $^{\#\#}P < 0.01$ and $^{\#}P < 0.05$ versus WT BFT. $^{**}P < 0.01$ and $^{*}P < 0.05$ compared with TG CTL (two-way ANOVA followed by Tukey multiple comparisons test). (**G**) Assessment of DRP1 immunoreactivity in the ventral horn of the lumbar spinal cord of WT and TG mice fed control or BFT diets. Insets correspond to high magnification images of DRP1 immunoreactivity in individual motor neurons. The expression of DRP1 was elevated in untreated P301S TG mice compared with WT mice with or without BFT. DRP1 immunoreactivity was robustly decreased by BFT treatment. Scale bar: 100 μm at low magnification and 25 μm at high magnification.

Material, Fig. S3C). Protein carbonyl levels were significantly elevated in P301S TG mice on a control diet relative to their WT littermates ($P < 0.05$) but were reduced in TG mice given BFT treatment. Lastly, mRNA levels of HO1, a putative marker of oxidative injury, were assessed (Supplementary Material, Fig. S3D). Enhanced levels of HO1 have been reported in patients with corticobasal degeneration and Pick's disease (37). Consistently, our findings demonstrated a marked increase in HO1 mRNA levels in P301S TG mice, which were significantly reduced following BFT administration.

BFT mitigates the inflammatory response

As a consequence of innate immune activation, increased levels of proinflammatory mediators have been reported in neurodegenerative disorders. Upregulated iNOS expression has been described in postmortem brain specimens of AD subjects. Herein, we investigated the effects of BFT on iNOS levels (Fig. 7A; Supplementary Material, Fig. S4A). Fluorescence confocal images depicted an elevated iNOS immunoreactivity within spinal cord motor neurons of TG mice on a control diet (Fig. 7A2). Exposure to BFT resulted in a significant reduction of iNOS expression in P301S mice (Fig. 7A5). Quantification of iNOS fluorescence intensity (Fig. 7B, $P < 0.01$) and mRNA levels (Fig. 7C, $P < 0.01$) showed significant decreases. We also examined the effects of BFT on the expression of other inflammatory mediators (Fig. 7D–I; Supplementary Material, Fig. S4B and C). Our findings showed that BFT treatment induced a significant decrease in COX-2 (Fig. 7E, $P < 0.05$), TNF-α (Fig. 7F, $P < 0.05$), IL-1β (Fig. 7H, $P < 0.05$), and NF-κB p65 (Fig. 7I, $P < 0.01$) immunoreactivity in motor neurons of the spinal cord in P301S TG mice compared with TG mice on control diet.

BFT stimulates the Nrf2/ARE pathway

The Nrf2/ARE signaling pathway has a pivotal role in the regulation of genes involved in detoxication of ROS and cytotoxic electrophiles. The Nrf2/ARE transcriptional pathway increases

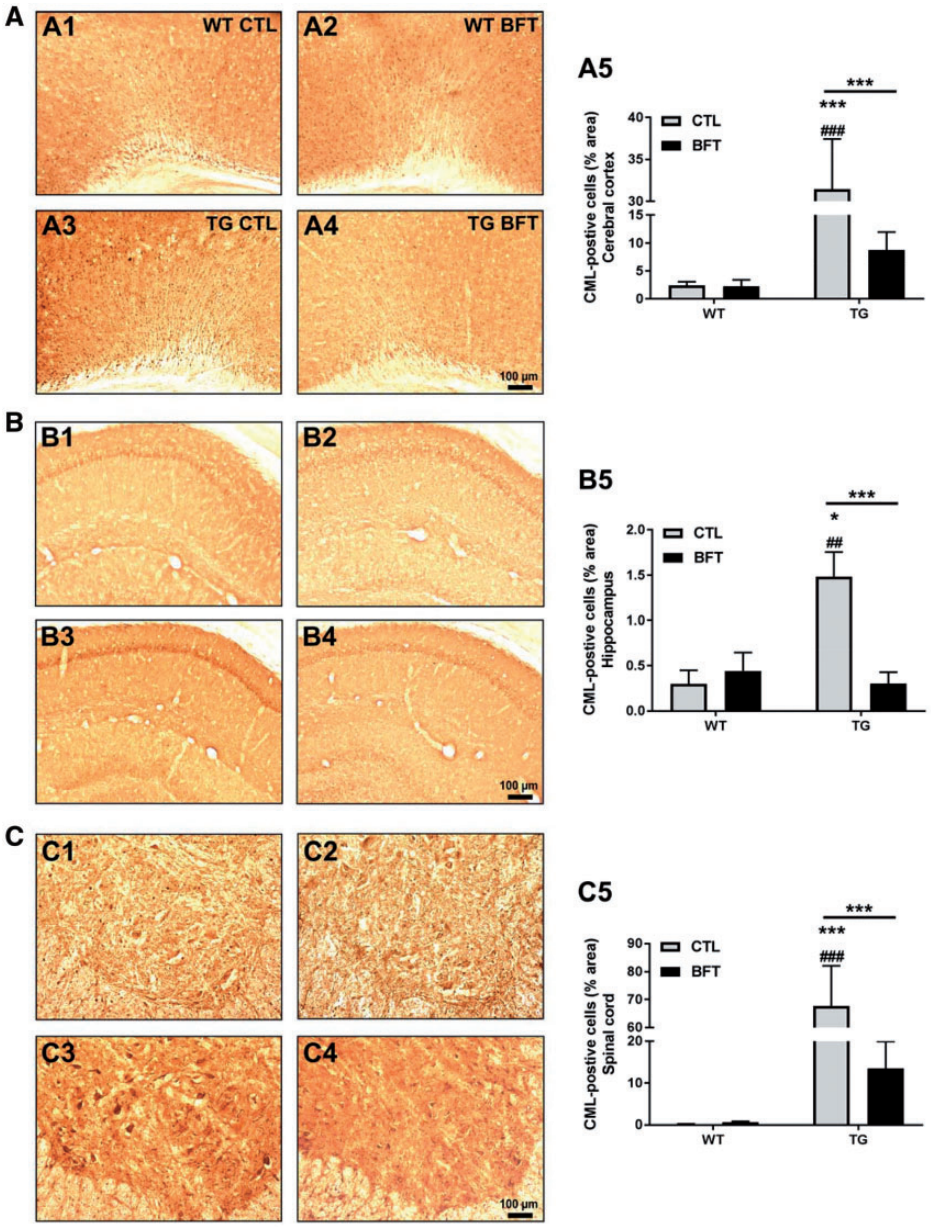

Figure 5. Exposure to BFT prevents the formation of AGEs. CML immunoreactivity in the cerebral cortex (**A**), hippocampus (**B**) and spinal cord (**C**) of WT and TG mice with or without BFT treatment. There was a substantial decrease in the percent area occupied by CML-immunoreactive cells following BFT exposure in P301S TG mice. WT, n = 3–5; TG, n = 7–10. $^{***}P < 0.001$ and $^{*}P < 0.05$ versus WT CTL. $^{###}P < 0.001$ and $^{##}P < 0.01$ compared with WT BFT. $^{***}P < 0.001$ relative to TG CTL (two-way ANOVA followed by Tukey multiple comparisons test). Scale bar: 100 µm.

protein chaperones, antioxidant enzymes and glutathione synthesis, and reduces COX-2 and iNOS (38,39). We therefore examined whether BFT could activate the Nrf2/ARE pathway in WT and Nrf2-deficient fibroblasts (Fig. 8). BFT administration induced transcription of four prototypical genes controlled by the Nrf2/ARE pathway: GSR, HO1, GCLM and NQO1 in WT but not in Nrf2 knock-out (KO) mouse embryonic fibroblasts (MEFs) (Fig. 8A). WT MEFs treated with 100 µM BFT for 3 h had significantly increased GSR and HO1 mRNA levels. Addition of 50 or 100 µM BFT for 8 h elevated GCLM and NQO1 mRNA levels compared with WT MEFs treated with vehicle, which remained unchanged in Nrf2 KO MEFs. None of the genes examined showed a response to thiamine except for GSR at the highest dose (100 µM) after 8 h treatment (Fig. 8B). These findings indicate that BFT can activate Nrf2/ARE genes in WT but not in Nrf2-deficient fibroblasts.

Neh2-luc reporter activation by BFT and its metabolites and docking studies

BFT is a chemical compound containing a phosphate moiety. In order to enter the cell, the phosphate moiety has to be removed by enzymatic reactions, which include alkaline phosphatase and ectonucleotidase enzymes. BFT decomposes to intermediary metabolites (that possess cellular permeability) and is ultimately converted into thiamine (40). These intermediary metabolites (s-BT and o-BT along with a plausible impurity z-

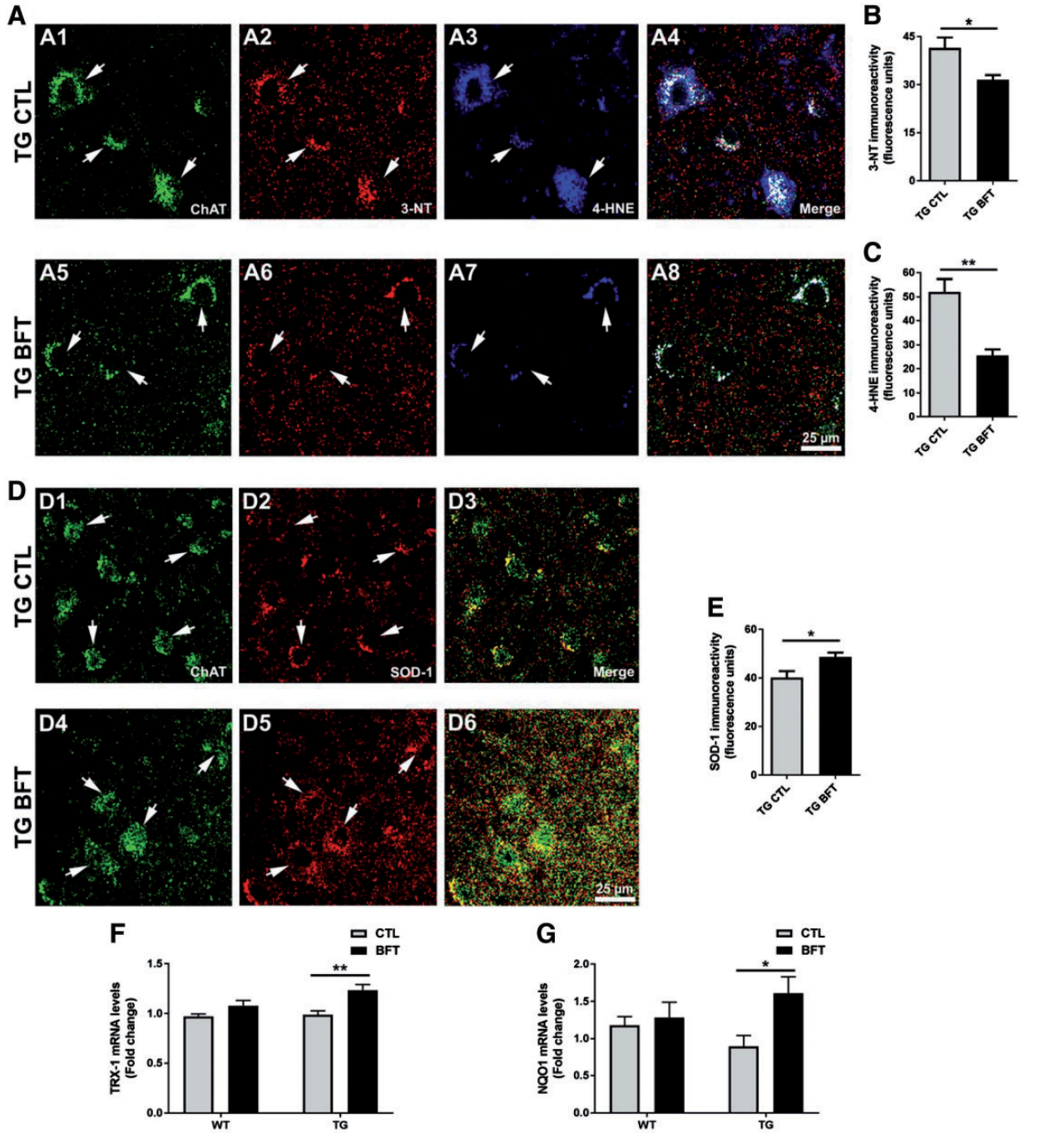

Figure 6. Dietary administration of BFT reduces oxidative and nitrosative stress. Representative ×40 confocal images for 3-NT and 4-HNE immunostaining in spinal cord sections (**A**). BFT treatment resulted in a significant decrease in the immunoreactivity of 3-NT and 4-HNE in P301S TG mice compared with TG mice on a control diet (**A2–A3** versus **A6–A7**, respectively). Quantification of fluorescence intensity for 3-NT (**B**) and 4-HNE (**C**). Histograms are representative of the average of 250–300 motor neurons corresponding to four to five sections per animal. Results are expressed as the mean ± S.E.M. of four to five mice per group. $^{**}P < 0.01$ and $^{*}P < 0.05$ compared with TG CTL (unpaired *t*-test). Scale bar: 25 µm. Immunofluorescent micrographs at ×40 depicted an enhanced expression of SOD-1 in TG mice treated with BFT relative to TG CTL mice (**D**). The mean fluorescence intensity signal for each ROI was determined in spinal cord sections, with data representing the average of 250–300 motor neurons corresponding to four to five sections per animal (**E**). Each group was comprised of four to five mice. $^{*}P < 0.05$ relative to TG CTL (unpaired *t*-test). Scale bar: 25 µm. Chronic administration of BFT upregulated mRNA levels of TRX-1 (**F**) and NQO1 (**G**) in P301S TG mice. A total of five to six mice from each genotype were used for quantitative analyses. $^{**}P < 0.01$ and $^{*}P < 0.05$ compared with TG CTL (two-way ANOVA followed by Tukey multiple comparisons test).

BT) were obtained from Hamari Chemicals (San Diego Research Center, SD, USA) and tested in a Neh2-luc *in vitro* reporter assay. The Neh2-luc reporter is a sensitive assay to monitor the direct effects of chemical entities which affect Nrf2 stability by modulating Nrf2/Keap1 and/or Keap–Cul3 interactions (41). BFT, s-BT, o-BT and z-BT (but not thiamine) showed potent activation of reporter activity in a dose-dependent manner in the 50–100 µM range (Fig. 8C). Interestingly, BFT metabolites showed more potent stimulation than BFT itself, with the activation effect decreasing in the order z-BT > o-BT = s-BT > BFT. We also tested

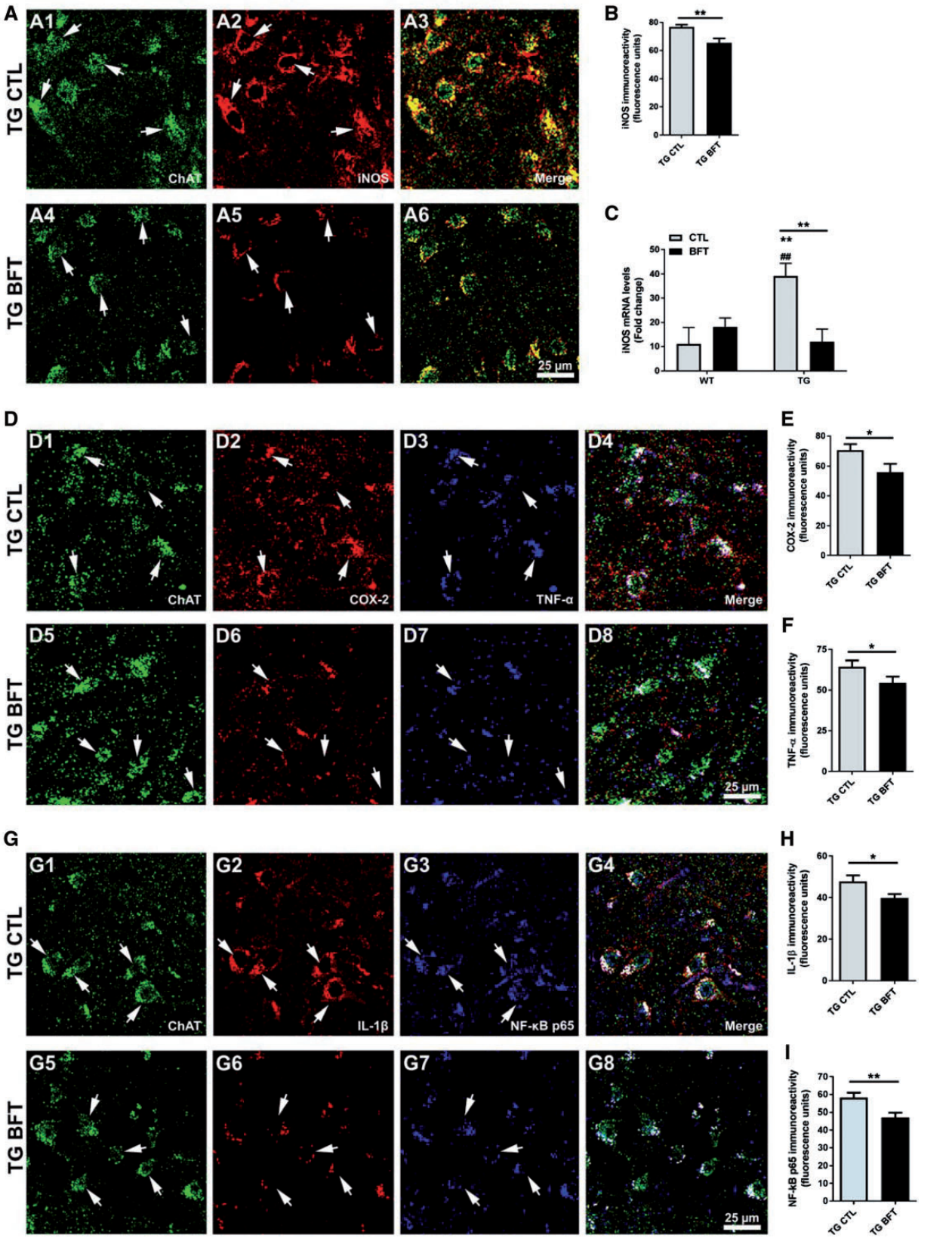

Figure 7. BFT treatment alleviates inflammation. (**A**) Confocal images depicted a marked iNOS immunoreactivity in TG CTL mice but oral administration of BFT significantly downregulated iNOS levels (**A2** versus **A5**). (**B**) Quantification of fluorescence levels of iNOS representative of the average of 250–300 motor neurons corresponding to four to five sections per animal. Results are expressed as the mean ± S.E.M. of four to five mice per group. $^{**}P < 0.01$ versus TG CTL (unpaired *t*-test). Scale bar: 25 µm. (**C**) Gene expression levels of iNOS in WT and TG mice fed either a control or BFT diet. Exposure to BFT caused a robust reduction in iNOS mRNA levels in P301S

these compounds in a hypoxia-inducible factor (HIF) ODD-luc reporter assay (Fig. 8D), where none of them showed significant luciferase activity, further confirming the specificity of their action on the Neh2-luc reporter. The concentration range for the observed Neh2-luc reporter activation by BFT and its metabolites is characteristic of that for Nrf2 activators working via the Nrf2 displacement mechanism: cell-permeable variants of the Nrf2 peptide activate the ARE-luc reporter with an EC_{50} of 75 μM (42). Small molecules such as NMBSA begin to activate the ARE-luc reporter only above 50 μM (43). The crystal structure for Keap1 bound NMBSA deposited to the Protein Data Bank (4IQK.pdb) was used in computer modeling. The Sum of energies (kcal/mol) scores obtained for BFT metabolites were in the order of z-BT > o-BT > s-BT > cz-BT > NMBSA (Supplementary Material, Table S2) and perfectly correlated with the order of Neh2-luc reporter activation. BFT metabolites show better scores when compared with NMBSA, suggesting that BFT metabolites can work via a displacement mechanism.

BFT and its metabolites activate Nrf2 driven ARE genes both in *in vitro* and *in vivo* systems

The reporter activation data were further confirmed by testing the ability of these molecules to trigger downstream ARE target genes in WT and Nrf2 KO MEFs. Similar to the Neh2-luc reporter activation, 100 μM BFT, s-BT, o-BT, and z-BT (but not thiamine) induced expression of downstream ARE genes including HO1, NQO1 and GCLM in WT MEFs (Fig. 8E) but no effect was seen in Nrf2 KO fibroblasts, thus showing the Nrf2 selectivity of the ARE response by these molecules. Thiamine, BFT and its metabolites were assessed *in vivo* for their ability to increase expression of genes known to be activated by the Nrf2/ARE transcription pathway. WT C57BL/6 mice were treated for 3 h with either vehicle or 1250 mg/kg of thiamine, BFT, s-BT, o-BT or z-BT through oral gavage and subjected to gene expression analysis. The active metabolites were more potent in activating the Nrf2 target genes than the parent molecule BFT (Fig. 8F).

Discussion

Reduced glucose metabolism (that may precede the onset of cognitive dysfunction by 10–15 years) occurs in a characteristic pattern in AD, corresponding to the default mode network (44), an area of reduced activity in the temporal-parietal cortex that preferentially succumbs to atrophy and Aβ deposition in AD (45). Glucose metabolism is strongly linked to thiamine-dependent pathways including the Krebs cycle and the pentose phosphate pathway, which are impaired in AD (5,6,13). Exposure to BFT improves cognitive impairment and reduces the amyloid burden in APP/PS1 TG mice in a dose-dependent fashion and was reported to diminish tau phosphorylation, which was attributed to decreased GSK-3β activity (26). Although BFT was reported to reduce tau phosphorylation in neurons in the APP/PS1 TG mice, tau phosphorylation has been previously observed in neurites of these mice (27,28).

We therefore examined the effects of BFT in P301S TG mice, which have a mutation in the human tau gene that is linked to frontotemporal dementia, and which develop early synaptic and behavioral impairments accompanied by the presence of NFTs, increased tau phosphorylation, mitochondrial abnormalities, oxidative damage and microglial activation (31,32,46). Chronic BFT treatment significantly improved the survival rate and behavioral deficits of the P301S TG mice. The reduced lifespan in P301S is accompanied by hind limb paralysis owing to the development of NFTs, and subsequent loss of motor neurons in the lumbar region of the spinal cord (32,33). Our findings demonstrate that BFT treatment significantly decreased the numbers of NFTs (hyperphosphorylated tau) in the cerebral cortex (∼65%) and hippocampus (∼60%) of P301S TG mice, and furthermore, it appeared to reduce NFTs in motor neurons which were protected against cell death.

After oral administration, BFT is hydrolyzed in the intestine into the lipophilic s-BT that diffuses across the epithelial membranes into the blood or liver, where it is converted into thiamine (40). As a result, blood thiamine concentrations reach 5-fold higher levels and persist longer than after administration of an equivalent dose of thiamine. Nevertheless, the magnitude of the rate of thiamine uptake into the brain is limited, in part, by a self-exchange mechanism catalyzed by the high affinity thiamine transporter (2). The present study is the first in which the effects of long-term BFT administration on brain thiamine and thiamine esters have been determined. We showed that BFT increased free thiamine, ThMP and ThDP levels in the liver and blood of P301S TG mice. Thiamine and ThMP levels were significantly elevated in the cerebral cortex and the hippocampus of WT mice whereas no changes were found in TG mice, and ThDP levels were variable between groups. Our findings are generally consistent with those of prior short-term studies (23,26,47).

Mitochondrial impairment is believed to cause or contribute to the development of both tau pathology and neurodegenerative diseases (19). Herein, we demonstrate that BFT treatment prevented the reduction in Complex I expression in the brains of P301S TG mice, although no alterations were observed in the other mitochondrial oxidative phosphorylation complexes. Reduced concentrations of thiamine in blood and decreased red blood cell TK activity are important indicators of thiamine deficiency. The coenzyme ThDP, which is associated with the direct oxidative pathway of glucose metabolism, increases TK activity in red blood cells (48). In the current study, administration of BFT significantly reversed the reduced TK activity in the cerebral cortex of P301S TG mice. The fact that we did not observe a consistent increase in brain ThDP levels suggests that enhanced TK activity may not be thiamine cofactor-mediated, or that our assay was not able to detect a slight but biologically important upregulation of ThDP (or another metabolite). It has recently been shown that TK is under Nrf2 control (49), which may very well account for the increase we observed. A number of studies

TG mice relative to TG CTL mice. $^{**}P < 0.01$ compared with WT CTL. $^{\#\#}P < 0.01$ versus WT BFT. $^{**}P < 0.01$ versus TG CTL (two-way ANOVA followed by Tukey multiple comparisons test). (**D**) Representative immunofluorescence confocal images at 40× for COX-2 and TNF-α in spinal cord sections. The immunoreactivity of COX-2 and TNF-α was significantly diminished in BFT-treated P301S TG mice relative to TG mice on a control diet (**D2–D3** versus **D6–D7**). Quantification of fluorescence intensity for COX-2 levels (**E**) and TNF-α (**F**). Each bar represents the mean ± S.E.M. of 250–300 motor neurons from four to five sections per animal. Each group was comprised of 4–5 mice. $^{*}P < 0.05$ compared with TG CTL (unpaired *t*-test). Scale bar: 25 μm. (**G**) Confocal micrographs at ×40 revealed that TG CTL mice displayed higher IL-1β and NF-κB p65 fluorescence intensity, which was substantially reduced following BFT treatment (**G2–G3** versus **G6–G7**). Quantification of immunofluorescence for IL-1β (**H**) and NF-κB p65 (**I**). All measurements are the average ± S.E.M. of 250–300 motor neurons from four to five sections per animal. Each group was comprised of four to five mice. $^{**}P < 0.01$ and $^{*}P < 0.05$ versus TG CTL (unpaired *t*-test). Scale bar: 50 μm at low magnification and 25 μm at high magnification.

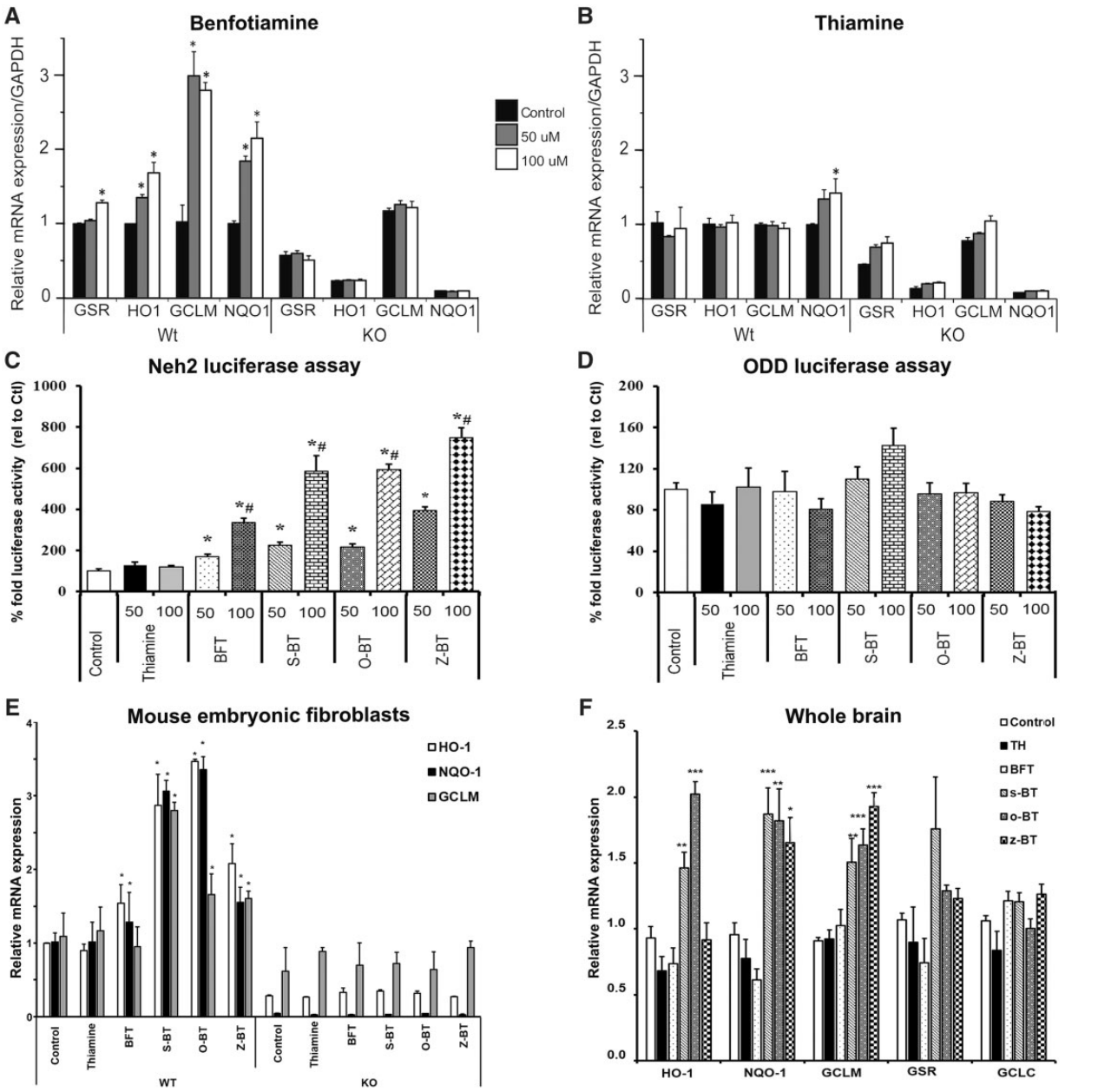

Figure 8. BFT and its metabolites activate the Nrf2/ARE pathway. BFT treatment induced transcription of Nrf2/ARE genes in WT but not Nrf2 KO MEFs. Nrf2 WT/KO MEFs were treated with solvent (Control, 1:1 pyridine:water) or 50 μM (50) or 100 μM (100) of either BFT (**A**) or thiamine (**B**). GSR and HO1 mRNA was measured after 3 h incubation with the drugs, where as GCLM and NQO1 were measured after 8 h of incubation. Thiamine did not have any effect on the genes examined except for GSR at the highest dose (100 μM) after 8 h treatment. Experiments were conducted in three biological replicates, each in six technical replicates. $^{*}P < 0.05$ when compared with WT control. (**C**) BFT, its metabolites and thiamine were tested for Neh2-luc activation (**C**) in Neh2-luc expressing SH-SY5Y cells and in ODD-luc assay (**D**) at two different concentrations (50 and 100 μM). BFT and its metabolites but not thiamine showed Neh2-luc activation whereas none of the compounds activated ODD-luc. The luciferase activity was measured and depicted as percentage fold activity. Data are mean ± S.E.M. from three independent experiments. $^{*}P < 0.05$ compared with control. $^{\#}P < 0.05$ relative to 50 μM of respective drug. (**E**) Effects of BFT and its metabolites on GCLM, NQO1 and HO1 ARE genes in Nrf2 WT and KO MEFs. The levels of mRNA were measured after 4 h of incubation with control (1:1, pyridine:water) or 100 μM of either thiamine, BFT, s-BT, o-BT or z-BT. Measurements were conducted at least three times for all conditions. $^{*}P < 0.05$ compared with WT control. (**F**) WT C57BL/6 mice were treated for 3 h with either vehicle or 1250 mg/kg of thiamine, BFT, s-BT, o-BT or z-BT through oral gavage. Gene expression changes were assessed by quantitative RT-PCR. All measurements are the averages ± S.E.M. from $n = $ five to six mice per group. $^{***}P < 0.001$, $^{**}P < 0.01$ and $^{*}P < 0.05$ relative to control. Statistical analyses were performed by two-way ANOVA with post hoc analysis by Dunnett's multiple comparison test.

have reported decreased expression and enzymatic activity of mitochondrial α-KGDHC in brain and fibroblasts of AD subjects (4,5). We found a reduction in the enzymatic activity of α-KGDHC in the frontal lobe of P301S TG mice, which was restored following BFT treatment.

To further investigate the relationship between mitochondrial dysfunction and tauopathy-related pathology, we focused on SOD-2, the main superoxide scavenger in mitochondria. Prior studies showed that a reduction in SOD-2 activity accelerated the onset of behavioral impairments, reduced dendritic

arborization and induced microglial activation in hAPP TG mice (50), and it increased amyloid burden and tau phosphorylation in the cerebral cortex of Tg2576 mice (51). In our study, P301S TG mice had decreased SOD-2 activity, which was restored by BFT administration. PGC-1α, which plays a pivotal role in controlling mitochondrial biogenesis and ROS suppression, has been implicated in the pathogenesis of several neurodegenerative disorders. The amount of PGC-1α mRNA is reduced in postmortem brain samples from AD, Parkinson's disease, and Huntington's disease patients when compared with age-matched controls (52–54). PGC-1α-mediated activation of mitochondrial biogenesis results from the co-activation of several transcription factors, including NRF1 and NRF2 (55). We found a decrease in the mRNA levels of PGC-1α in P301S TG mice, which were restored by BFT administration.

Mitochondrial DNA copy number is a surrogate marker of mitochondrial biogenesis. Systemic accumulation of somatic mtDNA regulatory control region mutations has been reported in the frontal cortex of AD and Down syndrome dementia subjects, with a resulting decrease in mtDNA copy number and mitochondrial function (56). In our study, BFT significantly increased mtDNA copy number by nearly 45% in TG mice. Moreover, mitochondrial dynamic processes are critical for the maintenance of mitochondrial morphology, autophagy and apoptosis. Alterations in the balance of fusion and fission events have emerged as a causal factor in neurodegeneration. The mitochondrial fission protein DRP1 is involved in several structural features of mitochondria, including shape, size and distribution and it plays a central role in mitophagy. An interaction between Aβ and DRP1 was seen in the cerebral cortex of AD patients and APP/PS1 TG mice (57). Mitochondrial elongation was found in neuronal populations of both Drosophila and TG mouse models of tauopathies owing to actin-mediated DRP1 mislocalization (58). A recent study in CRND8 APP mice showed that treatment with the mitochondrial fission inhibitor mdivi-1 rescued mitochondrial dynamics, reduced amyloid deposition and prevented cognitive deficits (59). We observed an increase in DRP1 levels in the P301S TG mice, which was reduced by BFT treatment.

Experimental evidence suggests that AGEs may contribute to neuronal dysfunction and death in both Parkinson's disease and AD (60). AGEs are present in senile plaques, NFTs and some granulovacuolar degeneration granules (61,62). The accumulation of AGEs in AD is associated with an acceleration of Aβ deposition and tau phosphorylation (63,64). Intracellular AGEs are colocalized with phosphorylated tau and it was suggested that they may precede NFTs and play a role in their formation (63–66). AGEs can activate RAGE, a receptor for Aβ, leading to GSK-3β activation that can phosphorylate tau (67). Interestingly, BFT can activate the pentose phosphate shunt by regulation of TK that results in the conversion of fructose-6-phosphate into pentose-5-phosphates and other sugars, preventing the formation of AGEs (24). In our study, BFT reduced the immunoreactivity of CML and tau hyperphosphorylation, consistent with a beneficial effect. The ability of BFT to activate glyoxalase 1 and reduce AGEs may directly contribute to its ability to decrease tau phosphorylation and NFTs.

A significant amount of evidence has demonstrated that oxidative stress contributes to tauopathy-related neurodegeneration. For instance, a marked accumulation of 8-hydroxy-2'-deoxyguanosine in mtDNA, protein carbonyl formation and tyrosine nitration have been detected in the frontal cortex and hippocampus of AD individuals at different stages of the disease (68). Enhanced oxidative stress is present in the frontal cortex, subthalamic nucleus and cerebellum of individuals with progressive supranuclear palsy (69–71). BFT administration for 2 weeks reduced diabetes-induced oxidized glutathione in the cerebral cortex of mice (72). In our study, BFT diminished 3-NT and 4-HNE immunoreactivity and protein carbonyls, and increased the levels of SOD and other redox proteins, such as TRX-1 and NQO1 in P301S TG mice.

There is evidence linking tau pathology in neurodegenerative diseases to inflammation. A substantial increase of several pro-inflammatory mediators, including iNOS, COX-2, TNF-α, IL-1β and NF-κB has been described in AD (73–75). We previously showed that reduced iNOS is beneficial and extends survival in the Tg2576 mouse model of AD (76). Prolonged and widespread activation of both astrocytes and microglial cells have been observed in tau-related disorders. Recently, it has been reported that the *SPI1* gene decreases the expression of the transcription factor PU.1, which regulates the expression of multiple AD-related genes in microglia and other myeloid cells, and delays the onset of AD (77,78). Glial activation closely correlates with the load and distribution of NFTs in P301S TG mice (32) and elevated levels of IL-1β and COX-2 as well as microglial activation have been observed in both the brain and spinal cord (79). BFT exhibits anti-inflammatory properties in LPS-stimulated cells (80,81). Consistent with prior studies, our findings here show that BFT exerts a potent anti-inflammatory effect in P301S TG mice, with reductions in iNOS, COX-2, TNF-α, IL-1β and NF-κB p65 levels.

The Nrf2/ARE transcriptional pathway is the master regulator of responses to oxidative stress, inflammation and mitochondrial dysfunction. Oxidative stress and/or exposure to electrophilic compounds cause the dissociation of the Nrf2-Keap1 complex. Nrf2 then translocates to the nucleus where it binds to AREs in the promoter regions of several genes involved in antioxidant and anti-inflammatory defenses. Nrf2 has beneficial effects on mitochondrial biogenesis and function (82). Activation of Nrf2 also downregulates iNOS and COX-2 and reduces AGEs formation through the transcriptional control of glyoxalase 1 (83). Nrf2 also increases expression of DNA repair enzymes and proteasome subunits. There is a reduction in Nrf2 levels in AD brains (84). Increased expression of Nrf2 in the hippocampus using a lentiviral vector improved learning and memory in APP/PS1 mice (85) while a deficiency of Nrf2 exacerbates AD-like pathology (86). We previously showed that activation of the Nrf2 pathway with triterpenoids was neuroprotective in TG mice with increased amyloid production (87). Activation of the Nrf2/ARE pathway attenuated tau-induced microgliosis in the hippocampus of mice expressing human P301L tau (88). We also demonstrated that methylene blue activates the Nrf2/ARE pathway and prevents tau-related neurotoxicity in the P301S TG mice (89) and that Nrf2 activating compounds fumarates increased glutathione synthesizing enzymes and protected against MPTP toxicity in WT but not in Nrf2 KO mice (90).

We therefore tested whether BFT and its metabolites are Nrf2 activators in both cells and in the mouse brain. Our data showed that BFT and its metabolites significantly increased the expression of Nrf2-dependent genes in WT but not in Nrf2-deficient fibroblasts as well as in brain, whereas thiamine had no effect. Moreover, the Neh2-luc reporter data indicate that both BFT and its metabolites (s-BT, o-BT and z-BT) are Nrf2 activators working via Nrf2 protein stabilization. The BFT metabolites were more potent in activating Nrf2 downstream genes than BFT *per se*. We cannot completely exclude the possibility of mild alkylating properties of these BFT metabolites; however, based on the high docking scores obtained in

comparison with those of NMBSA, it is likely that Nrf2 activation by BFT metabolites occurs by a displacement mechanism. This is advantageous since it avoids the potential toxicity of Nrf2 activators, which act by alkylation.

In summary, our study provides the first evidence that long-term treatment with BFT is neuroprotective in a mouse model of tauopathy. Many of the BFT-mediated beneficial effects observed in P301S TG mice may be attributable to activation of the Nrf2/ARE pathway. Active metabolites were more potent in activating the Nrf2 target genes than the parent molecule BFT. These findings demonstrate that BFT (and its metabolites) are of particular interest as potential treatments for neurodegenerative disorders in which tau pathology plays a pivotal role, including AD, frontotemporal dementia, progressive supranuclear palsy, Pick's disease, corticobasal degeneration and chronic traumatic encephalopathy.

Materials and Methods

Experimental design

All offspring were generated by breeding P301S TG male with wild-type (WT) female mice obtained from Jackson Laboratory (Bar Harbor, ME, USA), which had the same C57BL/6 ×C3H background. Animals were genotyped by PCR using genomic DNA extracted from mice tails. P301S TG mice and their WT littermates received either *ad libitum* control diet (LabDiet 5001) or diet containing 200 mg/kg/day of BFT (also known as *S*-benzoylthiamine *O*-monophosphate), which is the dose that produced the greatest efficacy in reducing the amyloid burden in APP/PS1 TG mice, although these authors administered BFT by gastric gavage daily for 8 weeks (26). In our experiments, mice were randomly classified into two groups: Cohort 1, assigned to survival assessment (mice were kept until natural death); Cohort 2, allocated to behavioral, histopathological, and biochemical analyses (mice were treated from 1 to 10 months). Behavioral tests were performed at 5, 7 and 9 months of age. Histopathological and biochemical analyses were conducted at 10 months of age. Both males and females were used equally (1:1 ratio); we did not find significant differences between them. All experiments were approved by the Animal Care and Use Committees of Weill Cornell Medicine and Augusta University.

Behavioral assessment

Anxiety was evaluated using a standard EPM test as previously described (31). The percentage of time spent in the open arms of the apparatus was calculated over the 5 min test. Emotional learning and memory were determined using contextual fear conditioning as described elsewhere (91). After the last shock, mice were left in the chamber for 30 s. Contextual fear memory was measured by scoring freezing behavior for 180 s when mice were placed back into the same conditioning chamber 24 h after training, using the FreezeFrame computerized system (Coulbourn Instruments, Allentown, PA, USA).

Tissue preparation

Half of the mice from each group were deeply anesthetized using sodium pentobarbital and transcardially perfused with ice-cold 0.9% sodium chloride and 4% paraformaldehyde (PFA). Tissue sections (40 μm-thick) were collected, post-fixed in 4% PFA followed by gradient sucrose (15 and 30%), and stored in cryoprotectant for immunohistochemical studies. The remaining mice in each group were sacrificed by decapitation; then, the brain and spinal cord were collected, snap frozen in liquid nitrogen, and stored at −80°C for subsequent analysis.

Neurochemistry

The levels of thiamine, ThDP and ThMP were measured using high-performance liquid chromatography (HPLC) with fluorescent detection in cerebral cortex, hippocampus, liver and blood on frozen samples as previously described (4).

Immunohistochemistry

Tissue sections for general histology were washed in phosphate-buffered saline (PBS) six times (10 min each) and treated with 3% hydrogen peroxide for 10 min. Following three PBS rinses, sections were blocked in 10% normal goat serum for 1 h, containing 0.3% Triton X-100. Next, tissue sections were incubated with primary antibodies (Supplementary Material, Table S1) for 24 h at 4°C. After three washes in PBS, sections were incubated at room temperature (RT) for 1 h in biotinylated secondary antibody (Supplementary Material, Table S1), rinsed again in PBS, and treated with avidin–biotin peroxidase complex solution (Vector, Burlingame, CA, USA). Tissue sections were visualized using diaminobenzidine and mounted directly onto slides using Aquamount.

Histological quantification was done using an average of four serial non-adjacent sections per animal (480 μm apart from bregma regions −1.34 through −2.84). The percent area occupied was measured within a 0.9-mm^2 area using Scion Image (Scion Corp., Frederick, MD, USA). For cerebral cortex, the measurements were made in an area encompassing the M1 (primary) and M2 (secondary) motor cortex regions with the threshold set at 50. For the hippocampus, the percent area occupied in the CA1 field was measured, using the dentate gyrus as an anatomical landmark, with the threshold set at 40.

For fluorescence analysis, tissue was removed from cryoprotectant and washed six times in PBS for 10 min each at RT. After blocking with a solution consisting in 10% normal donkey serum in PBS for 1 h, sections were incubated using primary antibodies (Supplementary Material, Table S1) in PBS with 1% normal donkey serum overnight at 4°C. Then, tissue sections were rinsed three times in PBS for 10 min each and subsequently incubated with conjugated secondary antibodies (Supplementary Material, Table S1) for 2 h. Lastly, after three washes in PBS for 10 min, the samples were mounted directly onto plus-coated slides and coverslipped using gelvatol mounting media.

Unbiased stereology

Spinal cord sections were mounted and immersed in 0.25% cresyl violet solution for 5 min. Quantification was done using eight serial non-adjacent sections per animal (240 μm apart from lumbar regions L3–L6). The number of motor neurons (>15 μm diameter) was estimated stereologically using the Optical Fractionator (Stereo Investigator, Microbrightfield, Burlington, VT, USA). The thickness of the sections was measured by focusing on the top of the section, setting the Z-axis to 0, and then refocusing to the bottom of the section. Analysis was carried out using a Nikon Plan Fluor 40× objective (NA 0.75) and only the cells with a visible nucleus were counted. The counting frame was 75× 75×14 μm (height×width×dissector

height) and the sampling grid was 150×150 μm. The average final section thickness was 20 μm, making the average guard zone 3 μm from the top and bottom of the section. An experimenter blinded to the treatment group performed all analyses.

Western blotting

Tissue was homogenized in ice-cold stringent radioimmunoprecipitation assay buffer (1:30, w/v, RIPA; 50 mM Tris–HCl, pH 8.0, with 150 mM sodium chloride, 1.0% Igepal CA-630 (NP-40), 0.5% sodium deoxycholate and 0.1% sodium dodecyl sulfate) containing the protease and phosphatase inhibitors by sonication. Proteins were quantified using the Bradford assay and lysates were either used immediately or stored at –80°C. Equal amounts of protein were electrophoresed through 4–20% Criterion TGX Gels (Bio-Rad Laboratories, Inc., Hercules, CA, USA). Polyvinylidene fluoride membranes were activated in 100% methanol. Protein was transferred to membranes and blocked in 5% BSA, 1× Tris-buffered saline (TBS), and 0.1% Tween-20 and exposed overnight to primary antibody (Supplementary Material, Table S1) in the same solution at 4°C. Membranes were then washed three times with TBST and incubated for 1 h with HRP-conjugated secondary antibody (Supplementary Material, Table S1). Immunoreactive proteins were detected using a chemiluminescent substrate (Pierce, ThermoFisher Scientific, Waltham, MA, USA) and analyzed using the NIH-based Scion Image software (Scion Corp, Frederick, MD, USA).

Gene expression analysis

Brain samples were processed for RNA extraction (Qiagen, Valencia, CA, USA). RT-PCR was performed using a SYBR Green-based assay on an ABI Prism 7900HT sequence detection system (Applied Biosystems, Foster City, CA, USA). Total messenger RNA was analyzed for the following genes: peroxisome proliferator-activated receptor gamma coactivator 1-alpha (PGC-1α), thioredoxin 1 (TRX-1), NAD(P)H dehydrogenase quinone 1 (NQO1), inducible nitric oxide synthase (iNOS), mitochondrial transcription factor A (TFAM), heme oxygenase 1 (HO1), glutathione reductase (GSR), gamma-glutamate-cysteine ligase modifier subunit (GCLM), gamma-glutamate-cysteine ligase catalytic subunit and glyceraldehyde 3-phosphate dehydrogenase (GAPDH, used as an internal control).

High-resolution confocal laser scanning microscopy analysis

Confocal microscopy was utilized to evaluate the oxidative stress and neuroinflammatory responses in the spinal cord of TG mice. Fluorescent images were acquired on a Leica TCS SP5 confocal microscope under constant power and pinhole aperture and evaluated using the LAS X software package. Fluorescence micrographs were obtained with an HCX PL APO CS40× (NA 1.25) oil-immersion objective lens. To quantitate protein levels, ROIs were outlined around the neuronal perikarya. Immunofluorescence intensity was determined for 3-nitrotyrosine (3-NT), 4-hydroxynonenal (4-HNE), SOD [SOD 1, peroxiredoxin 3 (PRDX3), iNOS, the enzyme cyclooxygenase 2 (COX-2), tumor necrosis factor-α (TNF-α), cytokine interleukin-1β (IL-1β) and nuclear factor kappa B (NF-kB) subunit p65].

Mitochondrial characterization

Frontal lobe samples (30–55 mg) were thawed on ice and dispersed using a 2-ml dounce homogenizer. The homogenate was centrifuged at 1000*g* ×5 min to get rid of nuclear fraction and cell debris. The resulting supernatant was centrifuged at 14 000*g*×5 min. The pellet was then collected and centrifuged again at 14 000*g*×5 min. The new obtained pellet was resuspended in 20 mM HEPES (pH 7.8) and used in any subsequent experiments. The protein lysates containing equal amounts of protein were separated by SDS-PAGE, electroblotted onto a nitrocellulose membrane (Bio-Rad, Hercules, CA, USA), and immunoreacted with an appropriate primary antibody followed by HRP conjugated secondary antibodies (Supplementary Material, Table S1). Immunoreactive proteins were visualized by incubating membranes in a chemiluminescence substrate (Pierce Biotechnology, Rockford, IL, USA) and analyzed using NIH Image J software.

Transketolase activity was determined with a coupled enzyme assay in which the glyceraldehyde phosphate product was isomerized to dihydroxyacetonephosphate and reduced with NADH (5). Alpha-ketoglutarate dehydrogenase (α-KGDHC) complex activity was monitored as the ketoglutarate dependent conversion of NAD^+ to NADH (α-ketoglutarate + NAD^+ + CoA → succinyl CoA + CO_2 + NADH) as previously described (5). SOD activity was assessed in semi-purified mitochondrial fraction (crude mitochondrial fraction, which may contain fragments of Endoplasmic Reticulum and microsomes, as it is technically impossible to eliminate these contaminants by standard differential centrifugation procedures) using an Enzo Life Sciences kit (#ADI-900-157). The succinate dehydrogenase (Complex II) and CS enzymatic activities were measured by well standardized, published methods (92,93). All activities and content values were normalized by protein content. The protein levels of NADH: ubiquinone oxidoreductase (Complex I, subunit NDUFB8), coenzyme Q reductase (Complex III, subunit Core 2), cytochrome c reductase (Complex IV, subunit MT-CO1) and ATP synthase (ATPase, subunit ATP5A1) were also quantitated by western blotting.

Mitochondrial DNA copy number

Tissues were processed for DNA extraction according to the Qiagen manufacturer's protocol (Valencia, CA, USA). The relative mtDNA copy number was determined by quantitative RT-PCR using the ratio of the mtDNA encoded subunit cytochrome oxidase 2 to the nuclear DNA encoded protein β-actin (94) on an ABI PRISM 7900H Sequence Detection System (Applied Biosystems) using the TaqMan Universal PCR Master mix and predeveloped TaqMan Gene Expression Assay primers/probes (Applied Biosystems). Threshold cycle values were expressed as the $2^{-\Delta Ct}$ of cytochrome oxidase.

Protein carbonyls

Carbonylated proteins were detected using an OxyBlot kit reagent (#10005020, Cayman Chemical, Ann Arbor, MI, USA). Carbonyl groups were derivatized to 2,4-dinitrophenylhydrazone (DNP-hydrazone) by reaction with 2,4-dinitrophenylhydrazine. The DNP-derivatized protein samples were separated by polyacrylamide gel electrophoresis followed by Western blotting. Next, immunodetection was performed with a primary antibody specific to the DNP moiety of the proteins and subsequent incubation with an HRP–antibody conjugate directed against the primary antibody. Blots were developed by using an enhanced

chemiluminescence method. Densitometric analysis of band intensity was used to quantitate protein oxidation.

Computer modeling

Docking experiments were performed using the CDOCKER algorithm, followed by force field minimization and binding energy calculations using the molecular mechanics algorithm CHARMm (as implemented in Discovery Studio 2.5, Accelrys, San Diego, CA, USA). The crystal structure of human Keap1 Kelch domain with the bound Nrf2 activator working via a displacement mechanism, *N,N′*-naphthalene-1,4-diylbis(4-methoxybenzenesulfonamide) or NMBSA (4IQK, docking scores and visualization of data are shown in Supplementary Material, Table S2) with hydrogen atoms added was the starting template structure. The docking control was performed with NMBSA: the molecule was placed into Keap1 exactly as observed in the crystal structure; the docking scores obtained for NMBSA were used for comparison. The docking experiments were done with the fixed constraints applied to the protein structure. The phosphate group of BFT was removed before docking owing to the known BFT *in vivo* activity only in the form of S-benzoylthiamine or *S*-(2-(*N*-((4-amino-2-methylpyrimidin-5-yl) methyl) formamido)-5-hydroxypent-2-en-3-yl) benzothioates-BT (s-BT, the negatively charged phosphate group will not penetrate the cell, moreover BFT will be dephosphorylated *in vivo* by enzymatic hydrolysis to s-BT). For z-BT ((Z)-S-(2-(*N*-((4-benzamido-2-methylpyrimidin-5-yl)methyl)formamido)-5-hydroxypent-2-en-3-yl)benzothioate)), docking was also determined for its cyclic form that will be generated *in vivo*, as cz-BT.

Luciferase reporter assays

Human neuroblastoma SH-SY5Y cells stably expressing Neh2- and ODD-luc reporters were plated at a density of 10 000 cells/well and cultured in DMEM/F12 medium supplemented with GlutaMAX, containing 10% FBS, 100 U/ml penicillin and 100 μg/ml streptomycin (38). Thiamine, BFT, s-BT, o-BT (*O*-benzoylthiamine or (3-[(4-amino-2-methyl-5-pyrimidinyl) methyl]-5-[2-(benzoyloxy) ethyl]-4-methyl-thiazolium) and z-BT were tested in 96-well plates at two different concentrations (50 and 100 μM) for 6 h. The number of cells was estimated using a Presto-Blue cell viability reagent (ThermoFisher Scientific). Next, the medium was removed, cells lysed, and luciferase activity was measured on a SpectraMax M5 Microplate Reader with BrightGlo reagent (Promega, Madison, WI, USA). The reporter activation was normalized to the background luminescence and the cell number. To demonstrate selectivity of Nrf2 activation, HIF-1 ODD-luc reporter assay was performed in the presence of BFT and its analogues, as previously described (38).

Nrf2-target genes assessment

Prototypical Nrf2 driven ARE genes were determined following administration of thiamine, BFT, s-BT, o-BT or z-BT at a single dose of 1250 mg/kg/day administered in 100 μl of vehicle [1% carboxymethyl cellulose solution in glycerol:water (60:40) mixture] by oral gavage. Control groups of mice received vehicle [1% carboxymethyl cellulose solution in glycerol:water (60:40) mixture] at the same volume. Mice were sacrificed, and the ventral midbrain and liver were collected after 3 h of drug administration and processed for RT-PCR analysis.

Fibroblast studies of gene expression

Both WT and Nrf2 KO MEFs were cultured in Isocove's Modified Dulbecco's Media supplemented with 10% FBS, 100 U/ml penicillin, and 100 μg/ml streptomycin in a humidified incubator set at 37°C with 5% CO_2 in six-well plates. Cells were treated with 100 μM of either vehicle (pyridine:water mixture; 1:1), thiamine, BFT, s-BT, o-BT or z-BT for a total incubation time of 4 h and harvested for real-time PCR. Total RNA (0.5 μg) was prepared using Trizol and reverse transcribed using a High Capacity Reverse Transcription kit (Life Technologies, Carlsbad, CA, USA). After dilution, 100 ng cDNA were used to measure relative gene expression compared with WT control. Specific primers and SYBR Select kit (Life Technologies) were used to amplify the cDNA in an ABI Prism 7900HT sequence detection system (Applied Biosystems). Relative gene expression was determined using the $^{\Delta\Delta}$Ct method with values normalized to GAPDH expression.

Statistical analysis

GraphPad Prism 7 software was utilized for statistical analysis, which was performed by two-way ANOVA followed by Tukey or Dunnett's post hoc test. Two-tailed unpaired *t*-test was used to compare only two groups (P301S mice fed either control or BFT diets). The cumulative survival was plotted using the Kaplan–Meier test. Data were expressed as mean ± S.E.M. A value of $P < 0.05$ was considered to be significant for all tests.

Supplementary Material

Supplementary Material is available at *HMG* online.

Acknowledgements

This work was supported by the NIA Grant P01AG014930 (G.E.G. and M.F.B.), NIH Grant R01-NS086746 (M.F.B.) and R01-NS101967 (B.T.), Tau Consortium/Rainwater Foundation (M.F.B.), National Parkinson Foundation (M.F.B., B.T.), Parkinson Support Group (B.T.) and Par fore Parkinson (B.T.). L.B. is Research Director of the Funds for Scientific Research (F.R.S.-FNRS, Belgium). J.V. was a Research Fellow of the 'Fonds pour la Formation à la Recherche dans l'Industrie et dans l'Agriculture' (F.R.I.A.).

Conflict of Interest statement. None declared.

References

1. Bettendorff, L. and Wins, P. (2009) Thiamin diphosphate in biological chemistry: new aspects of thiamin metabolism, especially triphosphate derivatives acting other than as cofactors. *FEBS J.*, **276**, 2917–2925.
2. Bettendorff, L. (1995) Thiamine homeostasis in neuroblastoma cells. *Neurochem. Int.*, **26**, 295–302.
3. Bettendorff, L., Mastrogiacomo, F., Kish, S.J. and Grisar, T. (2002) Thiamine, thiamine phosphates, and their metabolizing enzymes in human brain. *J. Neurochem.*, **66**, 250–258.
4. Gangolf, M., Czerniecki, J., Radermecker, M., Detry, O., Nisolle, M., Jouan, C., Martin, D., Chantraine, F., Lakaye, B. and Wins, P. (2010) Thiamine status in humans and content of phosphorylated thiamine derivatives in biopsies and cultured cells. *PLoS One*, **5**, e13616.
5. Gibson, G.E., Sheu, K.F., Blass, J.P., Baker, A., Carlson, K.C., Harding, B. and Perrino, P. (1988) Reduced activities of thiamine-dependent enzymes in the brains and peripheral

tissues of patients with Alzheimer's disease. *Arch. Neurol.*, **45**, 836–840.
6. Ke, Z.J. and Gibson, G.E. (2004) Selective response of various brain cell types during neurodegeneration induced by mild impairment of oxidative metabolism. *Neurochem. Int.*, **45**, 361–369.
7. Gold, M., Chen, M.F. and Johnson, K. (1995) Plasma and red blood cell thiamine deficiency in patients with dementia of the Alzheimer's type. *Arch. Neurol.*, **52**, 1081–1086.
8. Gold, M., Hauser, R.A. and Chen, M.F. (1998) Plasma thiamine deficiency associated with Alzheimer's disease but not Parkinson's disease. *Metab. Brain Dis.*, **13**, 43–53.
9. Molina, J.A., Jimenez-Jimenez, F.J., Hernanz, A., Fernandez-Vivancos, E., Medina, S., de Bustos, F., Gomez-Escalonilla, C. and Sayed, Y. (2002) Cerebrospinal fluid levels of thiamine in patients with Alzheimer's disease. *J. Neural Transm. (Vienna)*, **109**, 1035–1044.
10. Heroux, M., Raghavendra Rao, V.L., Lavoie, J., Richardson, J.S. and Butterworth, R.F. (1996) Alterations of thiamine phosphorylation and of thiamine-dependent enzymes in Alzheimer's disease. *Metab. Brain Dis.*, **11**, 81–88.
11. Mastrogiacoma, F., Bettendorff, L., Grisar, T. and Kish, S.J. (1996) Brain thiamine, its phosphate esters, and its metabolizing enzymes in Alzheimer's disease. *Ann. Neurol.*, **39**, 585–591.
12. Rao, V.L., Richardson, J.S. and Butterworth, R.F. (1993) Decreased activities of thiamine diphosphatase in frontal and temporal cortex in Alzheimer's disease. *Brain Res.*, **631**, 334–336.
13. Bubber, P., Haroutunian, V., Fisch, G., Blass, J.P. and Gibson, G.E. (2005) Mitochondrial abnormalities in Alzheimer brain: mechanistic implications. *Ann. Neurol.*, **57**, 695–703.
14. Karuppagounder, S.S., Xu, H., Shi, Q., Chen, L.H., Pedrini, S., Pechman, D., Baker, H., Beal, M.F., Gandy, S.E. and Gibson, G.E. (2009) Thiamine deficiency induces oxidative stress and exacerbates the plaque pathology in Alzheimer's mouse model. *Neurobiol. Aging*, **30**, 1587–1600.
15. Blass, J.P., Gleason, P., Brush, D., DiPonte, P. and Thaler, H. (1988) Thiamine and Alzheimer's disease. A pilot study. *Arch. Neurol.*, **45**, 833–835.
16. Meador, K., Loring, D., Nichols, M., Zamrini, E., Rivner, M., Posas, H., Thompson, E. and Moore, E. (1993) Preliminary findings of high-dose thiamine in dementia of Alzheimer's type. *J. Geriatr. Psychiatry Neurol.*, **6**, 222–229.
17. Nolan, K.A., Black, R.S., Sheu, K.F., Langberg, J. and Blass, J.P. (1991) A trial of thiamine in Alzheimer's disease. *Arch. Neurol.*, **48**, 81–83.
18. Calingasan, N.Y., Uchida, K. and Gibson, G.E. (1999) Protein-bound acrolein: a novel marker of oxidative stress in Alzheimer's disease. *J. Neurochem.*, **72**, 751–756.
19. Lin, M.T. and Beal, M.F. (2006) Mitochondrial dysfunction and oxidative stress in neurodegenerative diseases. *Nature*, **443**, 787–795.
20. Mouton-Liger, F., Rebillat, A.S., Gourmaud, S., Paquet, C., Leguen, A., Dumurgier, J., Bernadelli, P., Taupin, V., Pradier, L. and Rooney, T. (2015) PKR downregulation prevents neurodegeneration and beta-amyloid production in a thiamine-deficient model. *Cell Death Dis.*, **6**, e1594.
21. Calingasan, N.Y., Park, L.C., Calo, L.L., Trifiletti, R.R., Gandy, S.E. and Gibson, G.E. (1998) Induction of nitric oxide synthase and microglial responses precede selective cell death induced by chronic impairment of oxidative metabolism. *Am. J. Pathol.*, **153**, 599–610.
22. Hazell, A.S., Faim, S., Wertheimer, G., Silva, V.R. and Marques, C.S. (2013) The impact of oxidative stress in thiamine deficiency: a multifactorial targeting issue. *Neurochem. Int.*, **62**, 796–802.
23. Volvert, M.L., Seyen, S., Piette, M., Evrard, B., Gangolf, M., Plumier, J.C. and Bettendorff, L. (2008) Benfotiamine, a synthetic S-acyl thiamine derivative, has different mechanisms of action and a different pharmacological profile than lipid-soluble thiamine disulfide derivatives. *BMC Pharmacol.*, **8**, 10.
24. Hammes, H.P., Du, X., Edelstein, D., Taguchi, T., Matsumura, T., Ju, Q., Lin, J., Bierhaus, A., Nawroth, P. and Hannak, D. (2003) Benfotiamine blocks three major pathways of hyperglycemic damage and prevents experimental diabetic retinopathy. *Nat. Med.*, **9**, 294–299.
25. Balakumar, P., Rohilla, A., Krishan, P., Solairaj, P. and Thangathirupathi, A. (2010) The multifaceted therapeutic potential of benfotiamine. *Pharmacol. Res.*, **61**, 482–488.
26. Pan, X., Gong, N., Zhao, J., Yu, Z., Gu, F., Chen, J., Sun, X., Zhao, L., Yu, M. and Xu, Z. (2010) Powerful beneficial effects of benfotiamine on cognitive impairment and beta-amyloid deposition in amyloid precursor protein/presenilin-1 transgenic mice. *Brain*, **133**, 1342–1351.
27. Borchelt, D.R., Ratovitski, T., van Lare, J., Lee, M.K., Gonzales, V., Jenkins, N.A., Copeland, N.G., Price, D.L. and Sisodia, S.S. (1997) Accelerated amyloid deposition in the brains of transgenic mice coexpressing mutant presenilin 1 and amyloid precursor proteins. *Neuron*, **19**, 939–945.
28. Kurt, M.A., Davies, D.C., Kidd, M., Duff, K., Rolph, S.C., Jennings, K.H. and Howlett, D.R. (2001) Neurodegenerative changes associated with beta-amyloid deposition in the brains of mice carrying mutant amyloid precursor protein and mutant presenilin-1 transgenes. *Exp. Neurol.*, **171**, 59–71.
29. Arriagada, P.V., Growdon, J.H., Hedley-Whyte, E.T. and Hyman, B.T. (1992) Neurofibrillary tangles but not senile plaques parallel duration and severity of Alzheimer's disease. *Neurology*, **42**, 631–639.
30. Spires-Jones, T.L., Stoothoff, W.H., de Calignon, A., Jones, P.B. and Hyman, B.T. (2009) Tau pathophysiology in neurodegeneration: a tangled issue. *Trends Neurosci.*, **32**, 150–159.
31. Dumont, M., Stack, C., Elipenahli, C., Jainuddin, S., Gerges, M., Starkova, N.N., Yang, L., Starkov, A.A. and Beal, F. (2011) Behavioral deficit, oxidative stress, and mitochondrial dysfunction precede tau pathology in P301S transgenic mice. *FASEB J.*, **25**, 4063–4072.
32. Yoshiyama, Y., Higuchi, M., Zhang, B., Huang, S.M., Iwata, N., Saido, T.C., Maeda, J., Suhara, T., Trojanowski, J.Q. and Lee, V.M. (2007) Synapse loss and microglial activation precede tangles in a P301S tauopathy mouse model. *Neuron*, **53**, 337–351.
33. Lewis, J., McGowan, E., Rockwood, J., Melrose, H., Nacharaju, P., Van Slegtenhorst, M., Gwinn-Hardy, K., Paul Murphy, M., Baker, M., Yu, X. *et al.* (2000) Neurofibrillary tangles, amyotrophy and progressive motor disturbance in mice expressing mutant (P301L) tau protein. *Nat. Genet.*, **25**, 402–405.
34. Zhao, J., Sun, X., Yu, Z., Pan, X., Gu, F., Chen, J., Dong, W., Zhao, L. and Zhong, C. (2011) Exposure to pyrithiamine increases beta-amyloid accumulation, Tau hyperphosphorylation, and glycogen synthase kinase-3 activity in the brain. *Neurotox. Res.*, **19**, 575–583.
35. Tapias, V., Cannon, J.R. and Greenamyre, J.T. (2014) Pomegranate juice exacerbates oxidative stress and

nigrostriatal degeneration in Parkinson's disease. *Neurobiol. Aging*, **35**, 1162–1176.
36. Tapias, V., Hu, X., Luk, K.C., Sanders, L.H., Lee, V.M. and Greenamyre, J.T. (2017) Synthetic alpha-synuclein fibrils cause mitochondrial impairment and selective dopamine neurodegeneration in part via iNOS-mediated nitric oxide production. *Cell. Mol. Life Sci.*, **74**, 2851–2874.
37. Castellani, R., Smith, M.A., Richey, P.L., Kalaria, R., Gambetti, P. and Perry, G. (1995) Evidence for oxidative stress in Pick disease and corticobasal degeneration. *Brain Res.*, **696**, 268–271.
38. Kaidery, N.A., Banerjee, R., Yang, L., Smirnova, N.A., Hushpulian, D.M., Liby, K.T., Williams, C.R., Yamamoto, M., Kensler, T.W., Ratan, R.R. *et al.* (2013) Targeting Nrf2-mediated gene transcription by extremely potent synthetic triterpenoids attenuate dopaminergic neurotoxicity in the MPTP mouse model of Parkinson's disease. *Antioxid Redox Signal*, **18**, 139–157.
39. Stack, C., Ho, D., Wille, E., Calingasan, N.Y., Williams, C., Liby, K., Sporn, M., Dumont, M. and Beal, M.F. (2010) Triterpenoids CDDO-ethyl amide and CDDO-trifluoroethyl amide improve the behavioral phenotype and brain pathology in a transgenic mouse model of Huntington's disease. *Free Radic. Biol. Med.*, **49**, 147–158.
40. Hurt, J.K., Coleman, J.L., Fitzpatrick, B.J., Taylor-Blake, B., Bridges, A.S., Vihko, P. and Zylka, M.J. (2012) Prostatic acid phosphatase is required for the antinociceptive effects of thiamine and benfotiamine. *PLoS One*, **7**, e48562.
41. Smirnova, N.A., Haskew-Layton, R.E., Basso, M., Hushpulian, D.M., Payappilly, J.B., Speer, R.E., Ahn, Y.H., Rakhman, I., Cole, P.A., Pinto, J.T. *et al.* (2011) Development of Neh2-luciferase reporter and its application for high throughput screening and real-time monitoring of Nrf2 activators. *Chem. Biol.*, **18**, 752–765.
42. Steel, R., Cowan, J., Payerne, E., O'Connell, M.A. and Searcey, M. (2012) Anti-inflammatory effect of a cell-penetrating peptide targeting the Nrf2/Keap1 interaction. *ACS Med. Chem. Lett.*, **3**, 407–410.
43. Marcotte, D., Zeng, W., Hus, J.-C., McKenzie, A., Hession, C., Jin, P., Bergeron, C., Lugovskoy, A., Enyedy, I., Cuervo, H. *et al.* (2013) Small molecules inhibit the interaction of Nrf2 and the Keap1 Kelch domain through a non-covalent mechanism. *Bioorg. Med. Chem.*, **21**, 4011–4019.
44. Vlassenko, A.G., Vaishnavi, S.N., Couture, L., Sacco, D., Shannon, B.J., Mach, R.H., Morris, J.C., Raichle, M.E. and Mintun, M.A. (2010) Spatial correlation between brain aerobic glycolysis and amyloid-beta (Abeta) deposition. *Proc. Natl. Acad. Sci. USA.*, **107**, 17763–17767.
45. Bateman, R.J., Xiong, C., Benzinger, T.L., Fagan, A.M., Goate, A., Fox, N.C., Marcus, D.S., Cairns, N.J., Xie, X., Blazey, T.M. *et al.* (2012) Clinical and biomarker changes in dominantly inherited Alzheimer's disease. *N. Engl. J. Med.*, **367**, 795–804.
46. Takeuchi, H., Iba, M., Inoue, H., Higuchi, M., Takao, K., Tsukita, K., Karatsu, Y., Iwamoto, Y., Miyakawa, T., Suhara, T. *et al.* (2011) P301S mutant human tau transgenic mice manifest early symptoms of human tauopathies with dementia and altered sensorimotor gating. *PLoS One*, **6**, e21050.
47. Vignisse, J., Sambon, M., Gorlova, A., Pavlov, D., Caron, N., Malgrange, B., Shevtsova, E., Svistunov, A., Anthony, D.C., Markova, N. *et al.* (2017) Thiamine and benfotiamine prevent stress-induced suppression of hippocampal neurogenesis in mice exposed to predation without affecting brain thiamine diphosphate levels. *Mol. Cell Neurosci.*, **82**, 126–136.
48. Rossouw, J.E., Labadarios, D., Krasner, N., Davis, M. and Williams, R. (1978) Red blood cell transketolase activity and the effect of thiamine supplementation in patients with chronic liver disease. *Scand. J. Gastroenterol.*, **13**, 133–138.
49. Xu, I.M., Lai, R.K., Lin, S.H., Tse, A.P., Chiu, D.K., Koh, H.Y., Law, C.T., Wong, C.M., Cai, Z., Wong, C.C. *et al.* (2016) Transketolase counteracts oxidative stress to drive cancer development. *Proc. Natl. Acad. Sci. USA.*, **113**, E725–E734.
50. Esposito, L., Raber, J., Kekonius, L., Yan, F., Yu, G.Q., Bien-Ly, N., Puolivali, J., Scearce-Levie, K., Masliah, E. and Mucke, L. (2006) Reduction in mitochondrial superoxide dismutase modulates Alzheimer's disease-like pathology and accelerates the onset of behavioral changes in human amyloid precursor protein transgenic mice. *J. Neurosci.*, **26**, 5167–5179.
51. Melov, S., Adlard, P.A., Morten, K., Johnson, F., Golden, T.R., Hinerfeld, D., Schilling, B., Mavros, C., Masters, C.L., Volitakis, I. *et al.* (2007) Mitochondrial oxidative stress causes hyperphosphorylation of tau. *PLoS One*, **2**, e536.
52. Qin, W., Haroutunian, V., Katsel, P., Cardozo, C.P., Ho, L., Buxbaum, J.D. and Pasinetti, G.M. (2009) PGC-1alpha expression decreases in the Alzheimer disease brain as a function of dementia. *Arch. Neurol.*, **66**, 352–361.
53. Cui, L., Jeong, H., Borovecki, F., Parkhurst, C.N., Tanese, N. and Krainc, D. (2006) Transcriptional repression of PGC-1alpha by mutant huntingtin leads to mitochondrial dysfunction and neurodegeneration. *Cell*, **127**, 59–69.
54. Shin, J.H., Ko, H.S., Kang, H., Lee, Y., Lee, Y.I., Pletinkova, O., Troconso, J.C., Dawson, V.L. and Dawson, T.M. (2011) PARIS (ZNF746) repression of PGC-1alpha contributes to neurodegeneration in Parkinson's disease. *Cell*, **144**, 689–702.
55. Wu, Z., Puigserver, P., Andersson, U., Zhang, C., Adelmant, G., Mootha, V., Troy, A., Cinti, S., Lowell, B., Scarpulla, R.C. *et al.* (1999) Mechanisms controlling mitochondrial biogenesis and respiration through the thermogenic coactivator PGC-1. *Cell*, **98**, 115–124.
56. Coskun, P.E., Wyrembak, J., Derbereva, O., Melkonian, G., Doran, E., Lott, I.T., Head, E., Cotman, C.W. and Wallace, D.C. (2010) Systemic mitochondrial dysfunction and the etiology of Alzheimer's disease and down syndrome dementia. *J. Alzheimers Dis.*, **20**, S293–S310.
57. Manczak, M., Calkins, M.J. and Reddy, P.H. (2011) Impaired mitochondrial dynamics and abnormal interaction of amyloid beta with mitochondrial protein Drp1 in neurons from patients with Alzheimer's disease: implications for neuronal damage. *Hum. Mol. Genet.*, **20**, 2495–2509.
58. DuBoff, B., Gotz, J. and Feany, M.B. (2012) Tau promotes neurodegeneration via DRP1 mislocalization in vivo. *Neuron*, **75**, 618–632.
59. Wang, W., Yin, J., Ma, X., Zhao, F., Siedlak, S.L., Wang, Z., Torres, S., Fujioka, H., Xu, Y., Perry, G. and Zhu, X. (2017) Inhibition of mitochondrial fragmentation protects against Alzheimer's disease in rodent model. *Hum. Mol. Genet*, **26**, 4118–4131.
60. Vicente Miranda, H., Szego, E.M., Oliveira, L.M., Breda, C., Darendelioglu, E., de Oliveira, R.M., Ferreira, D.G., Gomes, M.A., Rott, R., Oliveira, M. *et al.* (2017) Glycation potentiates alpha-synuclein-associated neurodegeneration in synucleinopathies. *Brain*, **140**, 1399–1419.
61. Smith, M.A., Taneda, S., Richey, P.L., Miyata, S., Yan, S.D., Stern, D., Sayre, L.M., Monnier, V.M. and Perry, G. (1994) Advanced Maillard reaction end products are associated with Alzheimer disease pathology. *Proc Natl Acad Sci USA.*, **91**, 5710–5714.
62. Sasaki, N., Fukatsu, R., Tsuzuki, K., Hayashi, Y., Yoshida, T., Fujii, N., Koike, T., Wakayama, I., Yanagihara, R., Garruto, R. *et al.* (1998) Advanced glycation end products in Alzheimer's

disease and other neurodegenerative diseases. *Am. J. Pathol.*, **153**, 1149–1155.
63. Münch, G., Shepherd, C.E., McCann, H., Brooks, W.S., Kwok, J.B.J., Arendt, T., Hallupp, M., Schofield, P.R., Martins, R.N. and Halliday, G.M. (2002) Intraneuronal advanced glycation endproducts in presenilin-1 Alzheimer's disease. *Neuroreport*, **13**, 601–604.
64. Vitek, M.P., Bhattacharya, K., Glendening, J.M., Stopa, E., Vlassara, H., Bucala, R., Manogue, K. and Cerami, A. (1994) Advanced glycation end products contribute to amyloidosis in Alzheimer disease. *Proc. Natl. Acad. Sci. USA.*, **91**, 4766–4770.
65. Castellani, R.J., Harris, P.L., Sayre, L.M., Fujii, J., Taniguchi, N., Vitek, M.P., Founds, H., Atwood, C.S., Perry, G. and Smith, M.A. (2001) Active glycation in neurofibrillary pathology of Alzheimer disease: n (epsilon)-(carboxymethyl) lysine and hexitol-lysine. *Free Radic. Biol. Med.*, **31**, 175–180.
66. Yan, S.D., Yan, S.F., Chen, X., Fu, J., Chen, M., Kuppusamy, P., Smith, M.A., Perry, G., Godman, G.C., Nawroth, P., Zweier, J.L. and Stern, D. (1995) Non-enzymatically glycated tau in Alzheimer's disease induces neuronal oxidant stress resulting in cytokine gene expression and release of amyloid beta-peptide. *Nat. Med.*, **1**, 693–699.
67. Li, J., Liu, D., Sun, L., Lu, Y. and Zhang, Z. (2012) Advanced glycation end products and neurodegenerative diseases: mechanisms and perspective. *J. Neurol. Sci.*, **317**, 1–5.
68. Mecocci, P., MacGarvey, U. and Beal, M.F. (1994) Oxidative damage to mitochondrial DNA is increased in Alzheimer's disease. *Ann. Neurol.*, **36**, 747–751.
69. Albers, D.S., Augood, S.J., Martin, D.M., Standaert, D.G., Vonsattel, J.P. and Beal, M.F. (1999) Evidence for oxidative stress in the subthalamic nucleus in progressive supranuclear palsy. *J. Neurochem.*, **73**, 881–884.
70. Park, L.C., Albers, D.S., Xu, H., Lindsay, J.G., Beal, M.F. and Gibson, G.E. (2001) Mitochondrial impairment in the cerebellum of the patients with progressive supranuclear palsy. *J. Neurosci. Res.*, **66**, 1028–1034.
71. Schmid, U., Stopper, H., Heidland, A. and Schupp, N. (2008) Benfotiamine exhibits direct antioxidative capacity and prevents induction of DNA damage in vitro. *Diabetes Metab. Res. Rev.*, **24**, 371–377.
72. Wu, S. and Ren, J. (2006) Benfotiamine alleviates diabetes-induced cerebral oxidative damage independent of advanced glycation end-product, tissue factor and TNF-alpha. *Neurosci. Lett.*, **394**, 158–162.
73. Mrak, R.E. and Griffin, W.S. (2005) Potential inflammatory biomarkers in Alzheimer's disease. *J. Alzheimers Dis.*, **8**, 369–375.
74. Pasinetti, G.M. and Aisen, P.S. (1998) Cyclooxygenase-2 expression is increased in frontal cortex of Alzheimer's disease brain. *Neuroscience*, **87**, 319–324.
75. Vodovotz, Y., Lucia, M.S., Flanders, K.C., Chesler, L., Xie, Q.W., Smith, T.W., Weidner, J., Mumford, R., Webber, R. and Nathan, C. (1996) Inducible nitric oxide synthase in tangle-bearing neurons of patients with Alzheimer's disease. *J. Exp. Med.*, **184**, 1425–1433.
76. Nathan, C., Calingasan, N., Nezezon, J., Ding, A., Lucia, M.S., La Perle, K., Fuortes, M., Lin, M., Ehrt, S., Kwon, N.S. *et al.* (2005) Protection from Alzheimer's-like disease in the mouse by genetic ablation of inducible nitric oxide synthase. *J. Exp. Med.*, **202**, 1163–1169.
77. Huang, K.L., Marcora, E., Pimenova, A.A., Di Narzo, A.F., Kapoor, M., Jin, S.C., Harari, O., Bertelsen, S., Fairfax, B.P., Czajkowski, J. *et al.* (2017) A common haplotype lowers PU.1 expression in myeloid cells and delays onset of Alzheimer's disease. *Nat. Neurosci.*, **20**, 1052.
78. Huang, K.L., Marcora, E., Pimenova, A.A., Di Narzo, A.F., Kapoor, M., Jin, S.C., Harari, O., Bertelsen, S., Fairfax, B.P., Czajkowski, J. *et al.* (2017) A common haplotype lowers PU.1 expression in myeloid cells and delays onset of Alzheimer's disease. *Nat. Neurosci.*, **20**, 1052.
79. Bellucci, A., Westwood, A.J., Ingram, E., Casamenti, F., Goedert, M. and Spillantini, M.G. (2004) Induction of inflammatory mediators and microglial activation in mice transgenic for mutant human P301S tau protein. *Am. J. Pathol.*, **165**, 1643–1652.
80. Shoeb, M. and Ramana, K.V. (2012) Anti-inflammatory effects of benfotiamine are mediated through the regulation of the arachidonic acid pathway in macrophages. *Free Radic. Biol. Med.*, **52**, 182–190.
81. Yadav, U.C., Kalariya, N.M., Srivastava, S.K. and Ramana, K.V. (2010) Protective role of benfotiamine, a fat-soluble vitamin B1 analogue, in lipopolysaccharide-induced cytotoxic signals in murine macrophages. *Free Radic. Biol. Med.*, **48**, 1423–1434.
82. Dinkova-Kostova, A.T. and Abramov, A.Y. (2015) The emerging role of Nrf2 in mitochondrial function. *Free Radic. Biol. Med.*, **88**, 179–188.
83. Xue, M., Rabbani, N., Momiji, H., Imbasi, P., Anwar, M.M., Kitteringham, N., Park, B.K., Souma, T., Moriguchi, T., Yamamoto, M. *et al.* (2012) Transcriptional control of glyoxalase 1 by Nrf2 provides a stress-responsive defence against dicarbonyl glycation. *Biochem. J.*, **443**, 213–222.
84. Ramsey, C.P., Glass, C.A., Montgomery, M.B., Lindl, K.A., Ritson, G.P., Chia, L.A., Hamilton, R.L., Chu, C.T. and Jordan-Sciutto, K.L. (2007) Expression of Nrf2 in neurodegenerative diseases. *J. Neuropathol. Exp. Neurol.*, **66**, 75–85.
85. Kanninen, K., Heikkinen, R., Malm, T., Rolova, T., Kuhmonen, S., Leinonen, H., Yla-Herttuala, S., Tanila, H., Levonen, A.L., Koistinaho, M. *et al.* (2009) Intrahippocampal injection of a lentiviral vector expressing Nrf2 improves spatial learning in a mouse model of Alzheimer's disease. *Proc. Natl. Acad. Sci. USA.*, **106**, 16505–16510.
86. Joshi, G., Gan, K.A., Johnson, D.A. and Johnson, J.A. (2014) Increased Alzheimer's disease-like pathology in the APP/PS1DeltaE9 mouse model lacking Nrf2 through modulation of autophagy. *Neurobiol. Aging*, **36**, 664–679.
87. Dumont, M., Wille, E., Calingasan, N.Y., Tampellini, D., Williams, C., Gouras, G.K., Liby, K., Sporn, M., Flint Beal, M., Lin, M.T. *et al.* (2009) Triterpenoid CDDO-methylamide improves memory and decreases amyloid plaques in a transgenic mouse model of Alzheimer's disease. *J. Neurochem.*, **109**, 502–512.
88. Lastres-Becker, I., Innamorato, N.G., Jaworski, T., Rabano, A., Kugler, S., Van Leuven, F. and Cuadrado, A. (2014) Fractalkine activates NRF2/NFE2L2 and heme oxygenase 1 to restrain tauopathy-induced microgliosis. *Brain*, **137**, 78–91.
89. Stack, C., Jainuddin, S., Elipenahli, C., Gerges, M., Starkova, N., Starkov, A.A., Jove, M., Portero-Otin, M., Launay, N., Pujol, A. *et al.* (2014) Methylene blue upregulates Nrf2/ARE genes and prevents tau-related neurotoxicity. *Hum. Mol. Genet.*, **23**, 3716–3732.
90. Ahuja, M., Ammal Kaidery, N., Yang, L., Calingasan, N., Smirnova, N., Gaisin, A., Gaisina, I.N., Gazaryan, I., Hushpulian, D.M., Kaddour-Djebbar, I. *et al.* (2016) Distinct Nrf2 signaling mechanisms of fumaric acid esters and their role in neuroprotection against 1-methyl-4-phenyl-1,2,3,6-tetrahydropyridine-induced experimental Parkinson's-like disease. *J. Neurosci.*, **36**, 6332–6351.

91. Kimura, R. and Ohno, M. (2009) Impairments in remote memory stabilization precede hippocampal synaptic and cognitive failures in 5XFAD Alzheimer mouse model. *Neurobiol. Dis.*, **33**, 229–235.
92. Shepherd, D. and Garland, P.B. (1969) The kinetic properties of citrate synthase from rat liver mitochondria. *Biochem. J.*, **114**, 597–610.
93. Veeger, C., Der Vartanian, D.V. and Zeylemaker, W.P. (1969) Succinate dehydrogenase. *Methods Enzymol.*, **13**, 81–90.
94. D'Aurelio, M., Vives-Bauza, C., Davidson, M.M. and Manfredi, G. (2010) Mitochondrial DNA background modifies the bioenergetics of NARP/MILS ATP6 mutant cells. *Hum. Mol. Genet.*, **19**, 374–386.